

GRBs and fundamental physics

Patrick Petitjean · F. Y. Wang · X. F. Wu ·
J. J. Wei

Received: date / Accepted: date

Abstract Gamma-ray bursts (GRBs) are short and intense flashes at the cosmological distances, which are the most luminous explosions in the Universe. The high luminosities of GRBs make them detectable out to the edge of the visible universe. So, they are unique tools to probe the properties of high-redshift universe: including the cosmic expansion and dark energy, star formation rate, the reionization epoch and the metal evolution of the Universe. First, they can be used to constrain the history of cosmic acceleration and the evolution of dark energy in a redshift range hardly achievable by other cosmological probes. Second, long GRBs are believed to be formed by collapse of massive stars. So they can be used to derive the high-redshift star formation rate, which can not be probed by current observations. Moreover, the use of GRBs as cosmological tools could unveil the reionization history and metal evolution of the Universe, the intergalactic medium (IGM) properties and the nature of first stars in the early universe. But beyond that, the GRB high-energy photons can be applied to constrain Lorentz invariance violation (LIV) and to test Einstein's Equivalence Principle (EEP). In this paper, we review the progress on the GRB cosmology and fundamental physics probed by GRBs.

Patrick Petitjean
Institut d'Astrophysique de Paris, 98bis Boulevard Arago 75014 Paris - France
E-mail: petitjean@iap.fr

F. Y. Wang
School of Astronomy and Space Science, Nanjing University, Nanjing 210093, China
Key Laboratory of Modern Astronomy and Astrophysics (Nanjing University), Ministry of Education, Nanjing 210093, China
Tel.: +86-25-89687505
Fax: +86-25-83635192
E-mail: fayinwang@nju.edu.cn

X. F. Wu
Purple Mountain Observatory, Chinese Academy of Sciences, Nanjing 210008, China
E-mail: xfwu@pmo.ac.cn

J. J. Wei
Purple Mountain Observatory, Chinese Academy of Sciences, Nanjing 210008, China
E-mail: jjwei@pmo.ac.cn

1 Introduction

Gamma-ray bursts (GRBs) are among the most powerful explosions in the Universe (Mészáros 2006; Zhang 2007; Gehrels et al. 2009; Kumar & Zhang 2015; Wang et al. 2015), which can be classified into two classes: long GRBs and short GRBs (Kouveliotou et al. 1993). Long GRBs are formed by collapses of massive stars, meanwhile the progenitors of short GRBs are mergers of compact stars (Woosley & Bloom 2006). The high luminosities of GRBs make them detectable out to high redshifts. Similar as type Ia supernova (SNe Ia), long GRBs can be treated as “relative standard candles” (i.e., Amati et al. 2002; Ghirlanda et al. 2004a; Liang & Zhang 2005). Due to the collapsar model, long GRBs can probe the high-redshift star formation rate. They also offer the exciting opportunity to detect the Population III (Pop III) stars, because massive Pop III stars can die as GRBs. The smooth spectra of GRB afterglow allow that properties of the intergalactic (IGM) absorption features could be extracted. The metal absorption lines make GRBs powerful sources to study the metal enrichment history. The clean damping wings of GRBs make them ideal tools to study the reionization of IGM and interstellar medium (ISM) properties of their hosts.

First, GRBs can act as the complementary tools to study dark energy and cosmic accelerating expansion. The SNe Ia can be observed when accreting white dwarf stars exceed the mass of the Chandrasekhar limit and explode. Thus they can be treated as ideal standard candles. However, the double white dwarfs merger model of SNe Ia challenges the precision of this standard candle. The accelerating expansion of Universe is discovered by two supernova groups (Riess et al. 1998; Perlmutter et al. 1999), which is attributed to the mysterious component — dark energy. Other observations, such as the cosmic microwave background (CMB) (Spergel et al. 2003), baryonic acoustic oscillations (BAO) (Eisenstein et al. 2005), X-ray gas mass fraction in galaxy clusters (Allen et al. 2004), and Hubble parameters (Jimenez et al. 2003; Wang & Wang 2014), also indicate that the expansion of universe is speeding up. But hitherto the highest redshift of SNe Ia is 1.914 (Jones et al. 2013). GRBs are promising tools to fill the gap between SNe Ia and CMB (Dai et al. 2004; Ghirlanda et al. 2004b; Liang & Zhang 2005; Ghirlanda et al. 2006; Wang & Dai 2006c; Wang et al. 2007; Schaefer 2007; Wang 2012). Fortunately, some luminosity correlations of GRBs have been used to standardize GRB energetics (i.e., Ghirlanda et al. 2004a; Xu et al. 2005; Liang & Zhang 2006; Firmani et al. 2005; Amati 2006; Amati et al. 2008; Liang et al. 2008).

The high-redshift ($z > 6$) star formation rate (SFR) measurement beyond the reach of present instruments, particularly at the faint end of the galaxy luminosity function. Long GRBs formed by the collapse of massive stars, provide a complementary tools for measuring the SFR (Totani 1997; Wijers et al. 1998; Bromm et al. 2002). Because the lifetimes of massive stars are short, the formation rate can be treated as their death rate. Surprisingly, the Swift data reveals that long GRBs are not tracing the SFR directly, instead implying some kind of additional evolution (Daigne et al. 2006; Le & Dermer 2007; Yüksel & Kistler 2007; Salvaterra & Chincarini 2007; Guetta & Piran 2007; Kistler et al. 2008; Campisi et al. 2010; Salvaterra et al. 2012). But the conversion factor between GRB rate and SFR is hard to determine. So the common method is relating the GRBs observed at low redshift to the SFR measurements and also considering the additional evolution of the GRB rate relative to the SFR. The SFR derived from GRBs seems to be

much higher than that obtained from high-redshift galaxy surveys (Kistler et al. 2008, 2009; Wang & Dai 2009; Wang 2013). The additional evolution term can be expressed as $(1+z)^\delta$ ($\delta \sim 0.5 - 1.5$) (Kistler et al. 2008; Robertson & Ellis 2012; Wang 2013). Many models have been proposed to explain this additional evolution, including metallicity evolution (Li 2008; Qin et al. 2010), GRBs from cosmic strings (Cheng et al. 2010), evolution of initial mass function (Wang & Dai 2011a; Xu & Wei 2008), evolution of luminosity function (Virgili et al. 2011; Yu et al. 2012). However, some studies claimed that there is no discrepancy between GRB rate and SFR (Elliott et al. 2012; Hao & Yuan 2013). The sample selection and adopted SFR are important. Theoretical model and observations of host galaxies both support that long GRBs could occur in low-metallicity environment (Woosley & Heger 2006; Mészáros 2006; Langer & Norman 2006; Stanek et al. 2006; Levesque 2014; Wang & Dai 2014b).

What are the dominant sources of metal enrichment? What is the metal enrichment history? The above two questions are the key questions of metal enrichment. The metal enrichment can change the star formation mode, from a high-mass (Pop III) mode to a low-mass dominated (Pop I/II) one, if the metal exceeds a ‘critical metallicity’ of $Z_{\text{crit}} \sim 10^{-4} Z_\odot$ (Bromm et al. 2001; Schneider et al. 2002, 2006). The metal enrichment history is also connected with the reionization history. Absorption lines of distant bright sources, such as GRBs or quasars, are main sources of information about the chemical properties of high-redshift Universe (Oh 2002; Furlanetto & Loeb 2003; Oppenheimer et al. 2009). GRBs have several advantages compared to traditional quasars (Bromm & Loeb 2007). First, because their progenitors are stellar mass black holes, so the number density drops much less precipitously than quasars at $z > 6$ (Fan et al. 2006). Second, the spectra of GRBs are smooth power laws, which allows to extract absorption lines. Several absorption lines have been extracted from the GRB spectra, such as two absorption lines (Si IV and Fe II) in the spectrum of GRB 090423 (Salvaterra et al. 2009).

In this paper, we review the cosmological implications of GRBs. Then in the following sections the gamma-ray bursts cosmology is reviewed: The second section is dedicated to luminosity correlations and cosmological constraints from GRBs. Section 3 discusses the capability of GRBs to reveal the high-redshift SFR. In section 4, the capability of GRBs to probe the metal enrichment history is discussed. The tests on fundamental physics with GRBs are reviewed in sections 5 and 6. The last section provides a summary and future prospect.

2 The luminosity correlations of GRBs and dark energy

In order to investigate the properties of dark energy, the relation between distance and redshift is needed, i.e., the expansion history of our universe. The best way to measure the redshift-distance relation is using standard candles, such as SNe Ia. To this end, many projects have been proposed to determine the distances of SNe Ia with exquisite accuracy. However, due to the limited luminosity of SN Ia, they can only be detected at low redshifts, i.e., $z < 2.0$. If we study the evolution of dark energy at large redshift range, high-redshift standard candle is needed. GRBs could be complementary probes of dark energy at high redshifts. Many attempts have been performed to standardize GRBs. But the observed energies of GRBs span a wide range. After considering the collimation effect, Frail et al. (2001) found

that the collimated energies of GRBs clustered around 5×10^{50} erg, which was confirmed by Bloom et al. (2003). Meanwhile, the collimated jet predicts that the appearance of an achromatic break in the afterglow light curve of GRBs (Rhoads 1997; Sari 1999), which is important to standardize the energetic of GRBs.

In this section, we first review luminosity correlations of GRBs. Then the progress on dark energy revealed by GRBs is discussed. Some reviews have discussed this topic (i.e., Ghirlanda et al. 2006; Dai & Wang 2007; Amati & Della Valle 2013).

2.1 The luminosity correlations of GRBs

The isotropic luminosity L and the energy E of GRBs with redshifts can be calculated by the peak flux and the fluence. For example, the isotropic luminosity is

$$L = 4\pi d_L^2 P_{\text{bolo}} \quad (1)$$

and the total isotropic energy is

$$E_{\text{iso}} = 4\pi d_L^2 S_{\text{bolo}} (1+z)^{-1}. \quad (2)$$

Here, P_{bolo} and S_{bolo} are the bolometric peak flux and fluence, respectively. In the classical scenario, the presence of a jet affects the afterglow light curve which presents an achromatic break. So the observation of the afterglow allows to estimate the jet opening angle θ_{jet} . So after the geometric correction, the collimated energy $E_\gamma = E_{\text{iso}} F_{\text{beam}}$, where $F_{\text{beam}} = 1 - \cos \theta_{\text{jet}}$ is the beaming factor. The peak flux and fluence are given over a wide variety of observed bandpasses, and with the wide range of redshifts which correspond to different range of energy bands in the rest frame of GRBs. So the K-correction is important (Bloom et al. 2001). P_{bolo} and S_{bolo} are derived from the differential energy spectrum $\Phi(E)$ as follows:

$$P_{\text{bolo}} = P \times \frac{\int_{1/(1+z)}^{10^4/(1+z)} E \Phi(E) dE}{\int_{E_{\text{min}}}^{E_{\text{max}}} \Phi(E) dE}, \quad (3)$$

$$S_{\text{bolo}} = S \times \frac{\int_{1/(1+z)}^{10^4/(1+z)} E \Phi(E) dE}{\int_{E_{\text{min}}}^{E_{\text{max}}} E \Phi(E) dE}, \quad (4)$$

with P and S being the observed peak energy and fluence in units of photons/cm²/s and erg/cm², respectively, and $(E_{\text{min}}, E_{\text{max}})$ the detection thresholds of the observing instrument. In general, the differential energy spectrum is described by band function (Band et al. 1993),

$$\Phi(E) = \begin{cases} AE^\alpha e^{-(2+\alpha)E/E_{\text{peak}}} & E \leq \frac{\alpha-\beta}{2+\alpha} E_{\text{peak}} \\ BE^\beta & \text{otherwise} \end{cases} \quad (5)$$

where α is the power-law index for photon energies below the break and β is the power-law index for photon energies above the break. Some differential energy

spectra of GRBs also show power-law spectra plus an exponential cutoff. In the standard flat Λ CDM model, the luminosity distance d_L can be expressed as

$$d_L(z) = (1+z) \frac{c}{H_0} \int_0^z \frac{dz'}{\sqrt{\Omega_M(1+z')^3 + \Omega_\Lambda}}. \quad (6)$$

There are several intrinsic luminosity correlations of GRBs are found, such as $L_{\text{iso}}-\tau_{\text{lag}}$ correlation (Norris et al. 2000), $L_{\text{iso}}-V$ correlation (Fenimore & Ramirez-Ruiz 2000), Amati correlation (Amati et al. 2002), Yonetoku correlation (Yonetoku et al. 2004), Ghirlanda correlation (Ghirlanda et al. 2004a), Liang-Zhang correlation (Liang & Zhang 2005) and Combo-correlation (Izzo et al. 2015).

Due to GRBs cover large redshift range, whether the correlations evolve with the redshift should be discussed. It's found that the slope of Amati correlation may vary with redshift significantly using a small sample of GRBs (Li 2007). Basilakos & Perivolaropoulos (2008) found no statistically significant evidence for redshift dependence of slopes in five correlations using 69 GRBs compiled by Schaefer (2007). Wang et al. (2011a) enlarge the GRB sample and test six GRB correlations. There is no statistically significant evidence for the evolution of the luminosity correlations with redshift is found. The slopes of correlations versus redshift are all consistent with zero at the 2σ confidence level. But Lin et al. (2015) found that the Amati correlation of low-redshift GRBs differs from that of high-redshift GRBs at more than 3σ confidence level, which is insensitive to cosmological models.

2.2 Constraints on dark energy and cosmological parameters

The classical method to constrain dark energy is through its influence on the expansion history of the universe, which can be extracted from the luminosity distance $d_L(z)$ and the angular diameter distance $d_A(z)$. In addition, the weak gravitational lensing, growth of large-scale structure, and redshift space distortion can also provide useful constraints on dark energy. Theoretical models can be tested using the classical χ^2 statistic. The typical way to probe dark energy from standard candles is as follows. With luminosity distance d_L in units of megaparsecs, the theoretically predicted distance modulus is

$$\mu = 5 \log(d_L) + 25. \quad (7)$$

The likelihood functions for the cosmological parameters can be determined from χ^2 statistics,

$$\chi^2(\Omega_M, \Omega_{DE}) = \sum_{i=1}^N \frac{[\mu_i(z_i, H_0, \Omega_M, \Omega_{DE}) - \mu_{0,i}]^2}{\sigma_{\mu_{0,i}}^2}, \quad (8)$$

where $\mu_{0,i}$ is the observed distance modulus, and $\sigma_{\mu_{0,i}}$ is the standard deviation. The confidence regions in the $\Omega_M - \Omega_{DE}$ plane can be derived through marginalizing the likelihood functions over H_0 (i.e., integrating the probability density $p \propto \exp(-\chi^2/2)$ for all values of H_0).

A lot of effort had been made to constrain cosmological parameters using GRBs since their cosmological origin was confirmed. Schaefer et al. (2003) obtained the first GRB Hubble diagram based on $L_{\text{iso}} - V$ correlation, and found

the mass density $\Omega_M < 0.35$ at the 1σ confidence level. After Ghirlanda et al. (2004a) found the Ghirlanda correlation, Dai et al. (2004) first used this correlation with 12 bursts and found the mass density $\Omega_M = 0.35 \pm 0.15$ at the 1σ confident level for a flat universe by assuming that some physical explanation comes into existence. Ghirlanda et al. (2004b) using 14 GRBs and SNe Ia obtained $\Omega_M = 0.37 \pm 0.10$ and $\Omega_\Lambda = 0.87 \pm 0.23$. Assuming a flat universe, the cosmological parameters were constrained to be $\Omega_M = 0.29 \pm 0.04$ and $\Omega_\Lambda = 0.71 \pm 0.05$ (Ghirlanda et al. 2004b). Wang & Dai (2006a) using the Liang-Zhang correlation to investigate the transition redshifts in different dark energy models via GRBs and SNe Ia, see also Wang & Dai (2006b). Di Girolamo et al. (2005) simulated different samples of gamma-ray bursts and found that Ω_M could be determined with accuracy $\sim 7\%$ with data from 300 GRBs. Meanwhile, many works have been done in this field, such as Mörtzell & Sollerman (2005), Bertolami & Silva (2006), Firmani et al. (2006), Li et al. (2008), Basilakos & Perivolaropoulos (2008), Wang (2008), Yu et al. (2009), Cardone et al. (2009), Qi & Lu (2010), Demianski & Piedipalumbo (2011), Demianski et al. (2011), and Wei et al. (2013).

Unfortunately, because of lack of low- z GRBs, the luminosity correlations has been obtained only from moderate- z GRBs. So the correlations are cosmology-dependent, i.e., the isotropic energy E_{iso} , collimation-corrected energy E_γ , and luminosity L_{iso} are as functions of cosmological parameters. This is the so-called ‘‘circularity problem’’ of GRBs. In the following, we discuss different methods to overcome this problem.

The first method is fitting the cosmological parameters and luminosity correlation simultaneously. Schaefer (2007) used 69 GRBs and five correlations to constrain cosmological parameters. Wang et al. (2007) also used 69 GRBs and other cosmological probes to constrain cosmological parameters. They make simultaneous uses of five luminosity indicators, which are correlations of $L_{\text{iso}} - \tau_{\text{lag}}$, $L_{\text{iso}} - V$, $E_{\text{peak}} - L_{\text{iso}}$, $E_{\text{peak}} - E_\gamma$, and $\tau_{\text{RT}} - L_{\text{iso}}$. After obtaining the distance modulus of each burst using one of these correlations, the real distance modulus can be calculated,

$$\mu_{\text{fit}} = \left(\sum_i \mu_i / \sigma_{\mu_i}^2 \right) / \left(\sum_i \sigma_{\mu_i}^{-2} \right), \quad (9)$$

where the summation runs from 1 – 5 over the correlations with available data, μ_i is the best estimated distance modulus from the i -th relation, and σ_{μ_i} is the corresponding uncertainty. The uncertainty of the distance modulus is

$$\sigma_{\mu_{\text{fit}}} = \left(\sum_i \sigma_{\mu_i}^{-2} \right)^{-1/2}. \quad (10)$$

When calculating constraints on cosmological parameters and dark energy, the normalizations and slopes of the five correlations are marginalized. The marginalization method is to integrate over some parameters for all of its possible values. The χ^2 value is

$$\chi_{\text{GRB}}^2 = \sum_{i=1}^N \frac{[\mu_i(z_i, H_0, \Omega_M, \Omega_{DE}) - \mu_{\text{fit},i}]^2}{\sigma_{\mu_{\text{fit},i}}^2}, \quad (11)$$

where $\mu_{\text{fit},i}$ and $\sigma_{\mu_{\text{fit},i}}$ are the fitted distance modulus and its error. In addition to GRBs, SNe Ia, CMB, BAO, X-ray gas mass fraction in galaxy clusters and

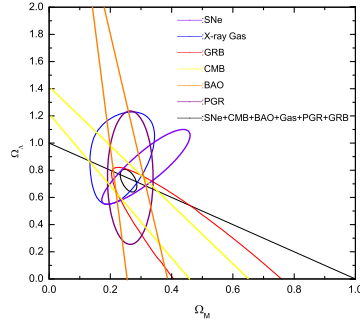


Fig. 1 Joint confidence intervals of 1σ for $(\Omega_M, \Omega_\Lambda)$ from the observational datasets. The thick black line contour, the blue contour, the red contour, the yellow contour, the violet contour, the orange contour, and the purple contour show constraints from from all the datasets, 26 galaxy clusters, 69 GRBs, CMB shift parameter, 182 SNe Ia, BAO, and 2dF Galaxy Redshift Survey, respectively. The thin solid line represents a flat universe. (Adapted from Figure 2 in Wang et al. (2007).)

growth rate data are also ideal cosmological probes. In Figure 1, the constraint on the Λ CDM model is shown. Different color contours represent constraints from different data. The best fitted parameters are consistent with a flat geometry. Li et al. (2008) also performed a Markov Chain Monte Carlo (MCMC) global fitting analysis to overcome the circularity problem. The Ghirlanda correlation and 27 GRBs are used. They treated the slopes of Ghirlanda correlation and cosmological parameters as free parameters and determine them simultaneously through MCMC analysis on GRB data together with other observational data, such as SNe Ia, CMB and large-scale structure (LSS). Amati et al. (2008) measured the cosmological parameters using Amati correlation using global fitting method. The extrinsic scatter was assumed on the parameter of E_{peak} , but the cosmological-dependent value is E_{iso} (Ghirlanda 2009).

The second method is to calibrate the correlations of GRBs using SNe Ia data at low redshifts. The principle of this method is that objects at the same redshift should have the same luminosity distance in any cosmology model. Therefore, the luminosity distance at any redshift in the redshift range of GRBs can be obtained by interpolating (or by other approaches) directly from the SNe Ia Hubble diagram. Then if further assuming these calibrated GRB correlations to be valid for all long GRB data, the standard Hubble diagram method to constrain the cosmological parameters from the GRB data at high redshifts obtained by utilizing the correlations. Liang et al. (2008) first calibrated the GRB correlations using an interpolation method. The error of distance modulus of linear interpolation can be calculated as (Liang et al. 2008; Wei 2010; Wei et al. 2015)

$$\sigma_\mu = \left(\left[\frac{z_{i+1} - z}{z_{i+1} - z_i} \right]^2 \epsilon_{\mu,i}^2 + \left[\frac{z - z_i}{z_{i+1} - z_i} \right]^2 \epsilon_{\mu,i+1}^2 \right)^{1/2}, \quad (12)$$

where $\epsilon_{\mu,i}$ and $\epsilon_{\mu,i+1}$ are errors of the SNe Ia, μ_i and μ_{i+1} are the distance moduli of the SNe Ia at z_i and z_{i+1} respectively. Similar to the interpolation method,

Cardone et al. (2009) constructed an updated GRBs Hubble diagram on six correlations calibrated by local regression from SNe Ia. Kodama et al. (2008) presented that the $L_{\text{iso}} - E_{\text{peak}}$ correlation can be calibrated with the empirical formula fitted from the luminosity distance of SNe Ia.

However, it must be noted that this calibration procedure depends seriously on the choice of the formula and various possible formulae can be fitted from the SNe Ia data that could give different calibration results of GRBs. As the cosmological constraints from GRBs are sensitive to GRBs calibration results (Wang 2008), the reliability of this method should be tested carefully. Moreover, as pointed out by Wang (2008), the GRB luminosity correlations which are calibrated by this way are no longer completely independent of all the SNe Ia data points. Therefore these GRB data can not be used to directly combine with the whole SNe Ia dataset to constrain cosmological parameters and dark energy. In order to search a unique expression of the fitting formula, Wang et al. (2009) used the cosmographic parameters (Capozziello & Izzo 2008; Vitagliano et al. 2010; Xia et al. 2012; Gao et al. 2012). The luminosity distance can be expanded as (Visser 2004)

$$d_L = \frac{c}{H_0} \left\{ z + \frac{1}{2}(1 - q_0)z^2 - \frac{1}{6}(1 - q_0 - 3q_0^2 + j_0)z^3 + \frac{1}{24} [2 - 2q_0 - 15q_0^2 - 15q_0^3 + 5j_0 + 10q_0j_0 + s_0] z^4 + O(z^5) \right\}, \quad (13)$$

where q is the deceleration parameter, j is the so-called ‘‘jerk’’, and s is the so-called ‘‘snap’’ parameter. These quantities are defined as

$$q = -\frac{1}{H^2} \frac{\ddot{a}}{a}; \quad (14)$$

$$j = \frac{1}{H^3} \frac{\dddot{a}}{a}; \quad (15)$$

$$s = \frac{1}{H^4} \frac{\ddddot{a}}{a}. \quad (16)$$

Equation (13) is only dependent on the cosmological principles and FRW metric, so the expansion is model-independent. But the Taylor-expansion of d_L is not valid at $z > 1$. So expansion d_L as a function of $y = z/1 + z$ is much useful (Wang & Dai 2011b). The calibrated Hubble diagram of GRBs is shown in Figure 2 (Wang & Dai 2011b).

The third method is to calibrate the standard candles using GRBs in a narrow redshift range (δz) near a fiducial redshift (Liang & Zhang 2006; Ghirlanda et al. 2006). Liang & Zhang (2006) proposed a procedure to calibrate the Liang-Zhang correlation with a sample of GRBs in a narrow redshift range. No low-redshift GRB sample is needed in this method. The calibration procedure can be described as follows. First, calibrate the power-law index of Liang-Zhang correlation using a sample of GRBs that satisfy this correlation and are distributed in a narrow redshift range. The power-law index can be derived using a multiple regression method. Second, marginalize the coefficient value over a reasonable range.

However, the gravitational lensing by random fluctuations in the intervening matter distribution induces a dispersion in GRB brightness (Oguri & Takahashi 2006; Schaefer 2007), degrading their value as standard candles as well as SNe Ia (Holz 1998). GRBs can be magnified (or reduced) by the gravitational lensing

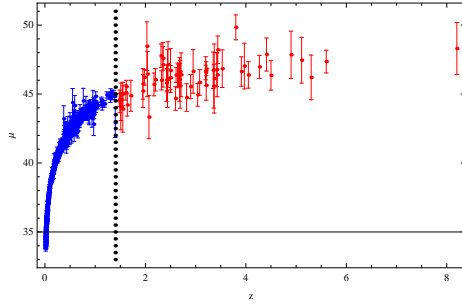


Fig. 2 The Hubble diagram of 557 SNe Ia (blue) and 66 high-redshift GRBs (red). (Adapted from Figure 2 in Wang & Dai (2011b).)

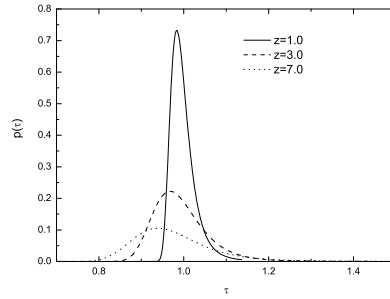


Fig. 3 Magnification probability distribution functions of gravitational lensing at redshifts $z = 1$, $z = 3$ and $z = 7$. (Adapted from Figure 5 in Wang & Dai (2011b).)

produced by the structure of the Universe. The gravitational lensing has sometimes a great impact on high-redshift GRBs. First, the probability distribution functions (PDFs) of gravitational lensing magnification have much higher dispersions and are markedly different from the Gaussian distribution (Valageas 2000; Oguri & Takahashi 2006; Wang & Dai 2011b). Figure 3 shows the magnification probability distribution functions of gravitational lensing at different redshifts (Wang & Dai 2011b). Second, there is effectively a threshold for the detection in the burst apparent brightness. With gravitational lensing, bursts just below this threshold might be magnified in brightness and detected, whereas bursts just beyond this threshold might be reduced in brightness and excluded. Wang & Dai (2011b) considered the weak lensing effect on cosmological parameters derived from GRBs, and found that the most probable value of the observed matter density Ω_M is slightly lower than its actual value, see Figure 4. The weak gravitational lensing also affects the dark energy equation of state by shifting it to a more negative value.

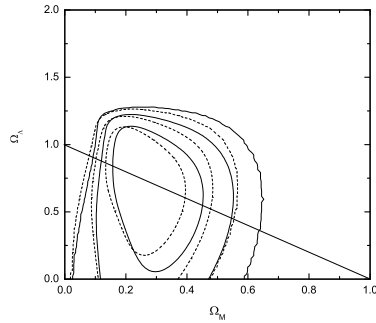


Fig. 4 Confidence contours of likelihood from 1σ to 3σ in the Λ CDM model. The black line contours from 116 GRBs and the dotted contours from 116 GRBs including magnification bias. (Adapted from Figure 7 in Wang & Dai (2011b).)

2.3 The equation of state of dark energy

The dark energy equation of state w is the most important parameter that describes the properties of dark energy. Whether and how it evolves with time is crucial for revealing the physics of dark energy. GRBs can provide the high-redshift evolution property of dark energy. The procedure is to bin w in z , and fit the w in each bin to observational data by assuming that w is constant in each bin. w_i is the EOS parameter in the i^{th} redshift bin defined by an upper boundary at z_i , and the zeroth bin is defined as $z_0 = 0$. Qi et al. (2008a) used GRBs and other cosmological observations to construct evolution of the equation of state, and found that the equation of state w is consistent with the cosmological constant (also see Qi et al. 2008b). The confidence interval of the uncorrelated equation of state parameter can be significantly reduced by adding GRBs. After calibrating the GRB correlations using cosmographic parameters, Wang & Dai (2011b) found that the high-redshift ($1.4 < z < 8.2$) equation of state is consistent with the cosmological constant. But some studies found that the equation of state w may deviate from -1 (i.e., Qi et al. 2009; Zhao et al. 2012). In light of the Planck CMB data, (Wang & Dai 2014a) found that the EOS is consistent with the cosmological constant at the 2σ confidence level, not preferring to a dynamical dark energy, which is shown in Figure 5.

3 The star formation rate and GRBs

3.1 Star formation rate derived from GRBs

The association of long GRBs with core-collapse supernovae has been confirmed from observations in recent years (Stanek et al. 2003; Hjorth et al. 2003), which provides a complementary technique for measuring the high-redshift SFR (Totani 1997; Wijers et al. 1998; Lamb & Reichart 2000; Porciani & Madau 2001; Bromm et al. 2002). The selection effects should be considered (for a review, see Coward 2007).

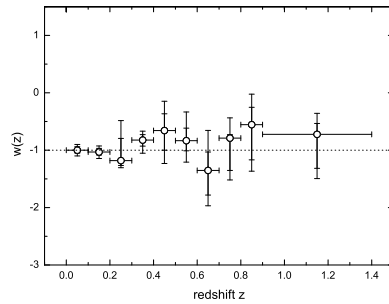


Fig. 5 Estimation of the uncorrelated dark energy EOS parameters at different redshift bins (w_1, w_2, \dots, w_{10}) from SNe Ia+BAO+WMAP9+H(z)+GRB data. The open points show the best fit value. The error bars are 1σ and 2σ confidence levels. The dotted line shows the cosmological constant. (Adapted from Figure 3 in Wang & Dai (2014a).)

But one crucial problem appears, i.e., how to calibrate the GRB event rate to the SFR. The luminosity function may play an important role (Natarajan et al. 2005; Daigne et al. 2006; Salvaterra & Chincarini 2007; Salvaterra et al. 2009; Campisi et al. 2010; Wanderman & Piran 2010; Cao et al. 2011). Before the launch of *Swift* (Gehrels et al. 2004), the luminosity function is determined by fitting the observed $\log N - \log P$ distribution (Schmidt 1999; Porciani & Madau 2001; Guetta et al. 2005; Natarajan et al. 2005). Thanks to the *Swift*, more redshifts of GRBs are measured. This makes it possible to give more information on the luminosity function (Wanderman & Piran 2010; Cao et al. 2011; Tan et al. 2013). Because the form of luminosity function should be assumed and the model parameters of luminosity function is degenerate, it is not easy to determine the luminosity function. A straightforward way to estimate the luminosity function is proposed by Lynden-Bell (1971) and then further developed by Efron & Petrosian (1992). This method has been used for GRBs (Lloyd-Ronning et al. 2002; Yonetoku et al. 2004; Wu et al. 2012). They found that the GRB rate is tracing SFR in a wide redshift range. But Yu et al. (2015) for the first time found that the GRB rate shows an unexpectedly low-redshift excess comparing to the observed SFR. In Figure 6, the blue stepwise line represents the comoving cosmic formation of GRBs as a function of redshift, and the error bar gives the 1σ confidence level. The best-fitting power laws for different segments are

$$\rho(z) \propto \begin{cases} (1+z)^{0.02 \pm 1.47} & z < 1.0, \\ (1+z)^{-0.35 \pm 0.70} & 1.0 < z < 4.0, \\ (1+z)^{-3.04 \pm 1.53} & z > 4.0. \end{cases} \quad (17)$$

The error bars are in the 95% confidence level. This result has been confirmed by later study by Petrosian et al. (2015). There are some possible reasons for this low-redshift excess.

The first one is that the definition of long GRBs is not clear. In classical method, the long GRBs are defined by $T_{90} > 2$ s (Kouveliotou et al. 1993). There is no clear boundary line in this diagram to separate the long and short GRBs. Moreover, T_{90} is an observed time scale, which represents different time for GRBs at different redshifts. Meanwhile, the observations of low-redshift long GRBs, such

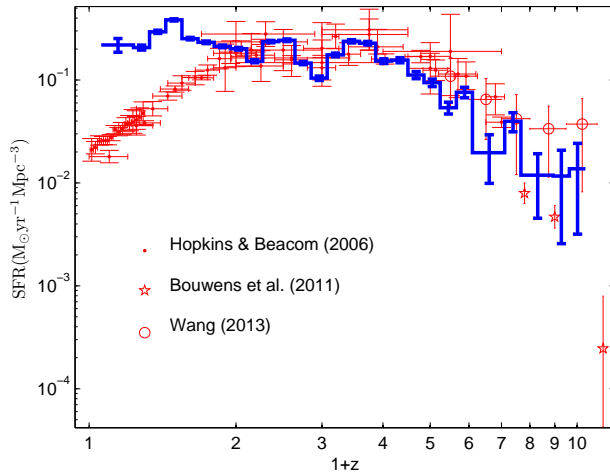


Fig. 6 The comparison between GRB formation rate $\rho(z)$ (blue) and the observed SFR. The SFR data are taken from Hopkins & Beacom (2006), which are shown as red dots. The SFR data from Bouwens et al. (2011) (stars) and Wang (2013) (open circles) are also used.

as GRB 060614 at $z = 0.125$ and GRB 060505 at $z = 0.089$, show no association of supernovae (Gal-Yam et al. 2006; Gehrels et al. 2006). So more physical criterions are required to classify GRBs. Because only a subclass of GRBs can trace the SFR. Some attempts have been performed (Zhang 2006; Zhang et al. 2009; Bloom et al. 2008). It has been suggested that GRBs can be classified physically into Type I (compact star origin) and Type II (massive star origin) (Zhang 2006, 2007).

The second one is that some selection effects have not been included in analysis. For example, it is easier to measure the redshift of those GRBs which are in lower redshift and therefore create a bias toward low redshift GRBs. It means that we lose some high redshift GRBs, so the formation rate of GRBs at low redshift we calculated will larger than the SFR.

The third one is that there may exist a subclass GRBs, i.e., low-luminosity GRBs (Cobb et al. 2006; Pian et al. 2006; Soderberg et al. 2006; Liang et al. 2007). The local rate of low-luminosity GRBs may be high, i.e., $\rho(0) = 100\text{--}1000 \text{ yr}^{-1} \text{ Gpc}^{-3}$ (Soderberg et al. 2006; Liang et al. 2007), much higher than high-luminosity GRBs. The progenitors of low-luminosity GRBs may be different with those of high-luminosity GRBs (Mazzali et al. 2006; Soderberg et al. 2006). The contamination from low-luminosity GRBs could lead to the low-redshift excess.

The expected redshift distribution of GRBs is

$$\frac{dN}{dz} = F(z) \frac{\varepsilon(z) \dot{\rho}_*(z) dV_{\text{com}}/dz}{\langle f_{\text{beam}} \rangle (1+z)}, \quad (18)$$

where $F(z)$ represents the ability to obtain the redshift, $\varepsilon(z)$ accounts for the fraction of stars producing GRBs, and $\dot{\rho}_*(z)$ is the SFR density. The $F(z)$ can be treated as constant when we consider the bright bursts with luminosities sufficient to be detected within an entire redshift range. GRBs that are unobservable due to beaming are accounted for through $\langle f_{\text{beam}} \rangle$. The $\varepsilon(z)$ can be parameterized as

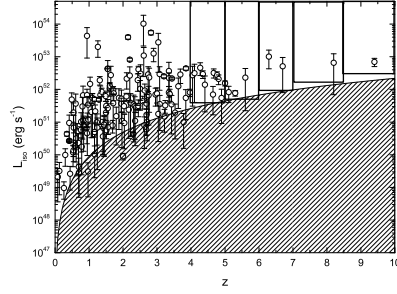


Fig. 7 Distribution of the isotropic-equivalent luminosity for 157 long-duration *Swift* GRBs. The shaded area approximates the detection threshold of *Swift* BAT. (Adapted from Figure 1 in Wang (2013).)

$\varepsilon(z) = \varepsilon_0(1+z)^\delta$, where ε_0 is an unknown constant that includes the absolute conversion from the SFR to the GRB rate in a given GRB luminosity range. Kistler et al. (2008) found the index $\delta = 1.5$ from 63 *Swift* GRBs. A little smaller value $\delta \sim 0.5 - 1.2$ has been inferred from update *Swift* GRBs (Kistler et al. 2009; Wang 2013). In a flat universe, the comoving volume is calculated by

$$\frac{dV_{\text{com}}}{dz} = 4\pi D_{\text{com}}^2 \frac{dD_{\text{com}}}{dz}, \quad (19)$$

where the comoving distance is

$$D_{\text{com}}(z) \equiv \frac{c}{H_0} \int_0^z \frac{dz'}{\sqrt{\Omega_m(1+z')^3 + \Omega_\Lambda}}. \quad (20)$$

In the calculations, the Λ CDM model with $\Omega_m = 0.27$, $\Omega_\Lambda = 0.73$ and $H_0 = 71 \text{ km s}^{-1} \text{ Mpc}^{-1}$ from the WMAP seven-year data is used (Komatsu et al. 2011).

Figure 7 shows the isotropic luminosity distribution of 157 *Swift* GRBs. The isotropic luminosity can be obtained by

$$L_{\text{iso}} = E_{\text{iso}}(1+z)/T_{90}, \quad (21)$$

where T_{90} is the duration time. The shaded area approximates the detection threshold of *Swift* BAT, which has a flux limit $\sim F_{\text{lim}} = 1.2 \times 10^{-8} \text{ erg cm}^{-2} \text{ s}^{-1}$. So the selection effect is important. In order to exclude faint low-redshift GRBs that could not be visible at high redshifts, we only select luminous bursts. The luminosity cut $L_{\text{iso}} > 10^{51} \text{ erg s}^{-1}$ is chosen in the redshift bin 0–4 (Yüksel et al. 2008), which removes many low-redshift, low-luminosity bursts that could not be detected at higher redshift. The cumulative distribution of GRB redshift can be expressed as

$$\frac{N(< z)}{N(< z_{\text{max}})} = \frac{N(0, z)}{N(0, z_{\text{max}})}. \quad (22)$$

The value of z_{max} is taken as 4.0. Because the SFR has been well measured at $z < 4.0$ (Hopkins & Beacom 2006). The theory predicted and observed cumulative

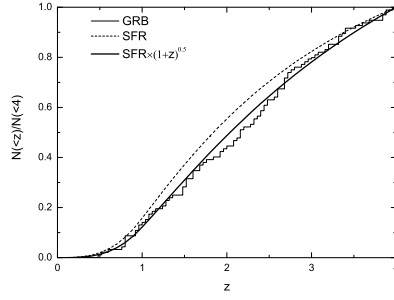


Fig. 8 Cumulative distribution of 92 *Swift* GRBs with $L_{\text{iso}} > 10^{51} \text{erg s}^{-1}$ in $z = 0 - 4$ (stepwise solid line). The dashed line shows the GRB rate inferred from the star formation history of Hopkins & Beacom (2006). The solid line shows the GRB rate inferred from the star formation history including $(1+z)^{0.5}$ evolution. (Adapted from Figure 2 in (Wang 2013).)

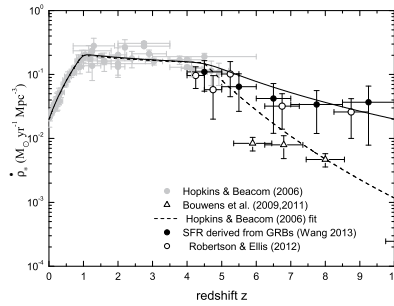


Fig. 9 The cosmic star formation history. The grey points are taken from Hopkins & Beacom (2006), the dashed line shows their fitting result. The triangular points are from Bouwens et al. (2009, 2011). The open circles are taken from (Robertson & Ellis 2012). The filled circles are the SFR derived from GRBs in (Wang 2013). (Adapted from Figure 3 in Wang (2013).)

GRB distributions is shown in Figure 8. The Kolmogorov-Smirnov statistic gives the minimization for $\delta = 0.5$ (Wang 2013).

The derived SFR from GRBs are shown as filled circles in Figure 9. Error bars correspond to 68% Poisson confidence intervals for the binned events (Gehrels 1986).

The formation rate of short GRBs is also extensively investigated. From the host galaxy and afterglow observations, it is believed that short GRBs originate from neutron star-neutron star or neutron star-black hole mergers (Berger 2014). So there is a delay time between the SFR and the merger rate, because the stellar evolution of binary stars and the binary orbits to spiral in. The delay time is about 3.0 Gyr (Wanderman & Piran 2015). The coalescence of a neutron star-neutron star is the mainly source of gravitational waves (GW). The simultaneous detection of a short GRB with a GW signal can constrain the nature of short GRBs. The

approximate detection horizon of neutron star-neutron star merger by Advanced LIGO/Virgo and other planned advanced GW detectors is about 300 Mpc.

3.2 Possible origins of high-redshift GRB rate excess

Recent studies show that the rate of GRBs does not strictly follow the SFH but is actually enhanced by some mechanism at high redshift (Le & Dermer 2007; Salvaterra & Chincarini 2007; Kistler et al. 2008; Yüksel et al. 2008; Wang & Dai 2009; Robertson & Ellis 2012; Wang 2013). The SFR inferred from the high-redshift ($z > 6$) GRBs seems to be too high in comparison with the SFR obtained from some high-redshift galaxy surveys (Bouwens et al. 2009, 2011).

3.2.1 Metallicity evolution

A natural origin of the high-redshift GRB rate excess is the metallicity evolution. Theory and observation both support that long GRBs prefer to occurring in low-metallicity environment. Some theoretical studies of long GRBs progenitors using stellar evolution models suggest that low metallicity may be a necessary condition for a long GRB to occur. For popular collapse models of long GRBs, stars with masses $> 30M_{\odot}$ can be able to create a black hole (BH) remnant (Woosley 1993; Hirschi et al. 2005). The preservation of high angular momentum and high-stellar mass at the time of collapse (Woosley 1993; MacFadyen & Woosley 1999) is crucial for producing a relativistic jet and high luminosity. Low-metallicity ($0.1 - 0.3Z_{\odot}$) progenitors can theoretically retain more of their mass due to smaller line-driven stellar winds (Kudritzki & Puls 2000; Vink & de Koter 2005), and hence preserve their angular momentum (Yoon & Langer 2005; Yoon et al. 2006), because the wind-driven mass loss of massive stars is proportional to the metallicity. Observations of long GRB host galaxies also show that they are typically in low metallicity environment, for several local long GRB host galaxies (Sollerman et al. 2005; Stanek et al. 2006), as well as in distant long GRB hosts (i.e., Fruchter et al. 2006; Prochaska et al. 2007).

Li (2008) studied the possibility of interpreting the observed discrepancy between the GRB rate history and the star formation rate history using cosmic metallicity evolution (Kistler et al. 2008). Under the assumption that the formation of long GRBs follows the cosmic star formation history and form preferentially in low-metallicity galaxies, the rate of GRB is given by

$$R_{\text{GRB}}(z) = k_{\text{GRB}}\Sigma(Z_{\text{th}}, z)\rho_*(z), \quad (23)$$

where k_{GRB} is the GRB formation efficiency, $\Sigma(Z_{\text{th}}, z)$ is the fraction of galaxies at redshift z with metallicity below Z_{th} (Langer & Norman 2006) and $\rho_*(z)$ is the observed SFR. The function $\Sigma(Z_{\text{th}}, z)$ is (Langer & Norman 2006)

$$\Sigma(Z_{\text{th}}, z) = \frac{\hat{\Gamma}[\alpha_1 + 2, (Z_{\text{th}}/Z_{\odot})^2 10^{0.15\beta z}]}{\Gamma(\alpha_1 + 2)}, \quad (24)$$

where $\hat{\Gamma}$ and Γ are the incomplete and complete gamma functions, $\alpha_1 = -1.16$ and $\beta = 2$ (Savaglio et al. 2005). Li (2008) found that the distribution of luminosity and cumulative distribution of redshift could be well fitted if $Z_{\text{th}} = 0.3Z_{\odot}$ is adopted.

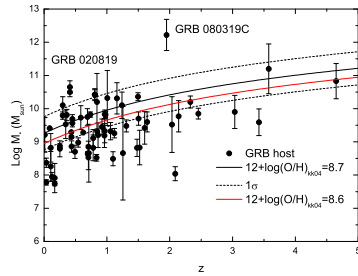


Fig. 10 GRB host galaxy mass distribution. The solid lines represent the upper limits of the stellar mass of a GRB host galaxy given a metallicity cutoff of $12+\log(\text{O}/\text{H})_{\text{K04}} = 8.7$ (black), and $12+\log(\text{O}/\text{H})_{\text{K04}} = 8.6$ (red). The dashed lines represent the 1σ scatter. (Adapted from Figure 4 in Wang & Dai (2014b).)

Wang & Dai (2009) studied the high-redshift SFR by considering the GRBs tracing the star formation history and the cosmic metallicity evolution. They found the SFR derived from GRBs is marginal consistent with that from traditional way (i.e., Hopkins & Beacom 2006). Wei et al. (2014) examined the influence on the GRB distribution due to the background cosmology, i.e., $R_h = ct$ Universe. However, a few GRB hosts with high metallicity are observed (i.e. GRB 020819), so that the role of metallicity in driving the GRB phenomena remains unclear and it is still debated (Price et al. 2007; Wolf & Podsiadlowski 2007; Kocevski et al. 2009; Graham et al. 2009; Svensson et al. 2010). For excellent reviews, see ? and Levesque (2014). But there are some uncertainties when measure the metallicities of GRBs’ explosion region at high-redshifts, such as chemical inhomogeneity (Levesque et al. 2010; Niino 2011). Wang & Dai (2014b) studied the metallicity role from two aspects, the GRB host galaxies and redshift distribution. They found that the observed GRB host galaxy masses and the cumulative redshift distribution can fit the predicted distributions well if GRBs occur in low-metallicity $12 + \log(\text{O}/\text{H})_{\text{K04}} < 8.7$, which is shown in Figure 10. Trenti et al. (2015) found that there is clear evidence for a relation between SFR and GRB (Jimenez & Piran 2013). But a sharp cut-off of metallicity is ruled out.

3.2.2 Evolving star initial mass function

Wang & Dai (2011b) proposed that the GRB rate excess may be due to the evolution of star initial mass function (IMF), also see Xu & Wei (2008). Because an “top-heavy” IMF will lead to more massive stars at high-redshift which can result in much more GRBs. Considering long GRBs trace SFR, the rate of GRBs in an evolving IMF is

$$R_{\text{GRB}} \propto \frac{N_{m>30M_{\odot}}}{V} = K \left(\frac{c}{H_0} \right)^{-3} \frac{\int_{30M_{\odot}}^{m_l} \xi(m) d \log m}{\int_{m_s}^{m_l} m \xi(m) d \log m} \rho_*(z), \quad (25)$$

where K is a constant to be constrained and R_{GRB} is the rate of GRBs, representing the number of GRBs per unit time per unit volume at redshift z . The evolving

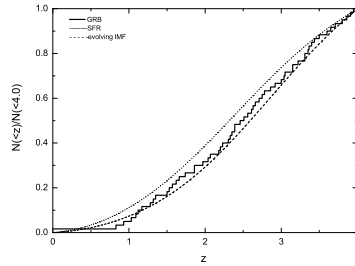


Fig. 11 The cumulative distribution of 72 *Swift* long GRBs with $L_{\text{iso}} > 0.8 \times 10^{51} \text{ erg s}^{-1}$ (stepwise solid line). The dotted line shows the GRB rate inferred from the star formation history of Hopkins & Beacom (2006). The dashed line shows the GRB rate inferred from star formation history including an evolving IMF. (Adapted from Figure 2 in Wang & Dai (2011b).)

IMF proposed by Davé (2008) is

$$\frac{dN}{d \log m} = \xi(m) \propto \begin{cases} m^{-0.3} & \text{for } m < \hat{m}_{\text{IMF}} \\ m^{-1.3} & \text{for } m > \hat{m}_{\text{IMF}}, \end{cases} \quad (26)$$

where $\hat{m}_{\text{IMF}} = 0.5(1+z)^2 M_{\odot}$, which has been constrained by requiring non-evolving star formation activity parameter. Figure 11 shows that the observed cumulative distribution of GRBs can be well produced by this model.

3.2.3 Evolving luminosity function break

Virgili et al. (2011) found that if the break of luminosity function evolves with redshift, the distributions of luminosity, redshift and peak photon flux from the BATSE and *Swift* data can be reproduced from simulations. The break luminosity function evolution can be in a moderate way $\propto L_b \times (1+z)^{\sim 0.8-1.2}$. Campisi et al. (2010) studied the luminosity function, the rate of long GRBs at high redshift, using high-resolution N-body simulations. A strongly evolving luminosity function with no metallicity cut may well explain the $\log N - \log P$ distribution of BATSE and *Swift* data.

3.2.4 Superconducting cosmic string

Cosmic strings are thought to be linear topological defects that could be formed at a phase transition in very early Universe. By considering that high-redshift GRBs 080913 and 090423 are electromagnetic bursts of superconducting cosmic strings, Cheng et al. (2010) showed the high-redshift GRB excess can be reconciled. But Wang et al. (2011b) claimed that GRBs from cosmic string have a very small angle, about 10^{-3} , which could be in contradiction with the opening angle of the GRB outflow. Cheng et al. (2011) pointed out that the angle is not the opening angle of the GRB outflow, but is just the collimation angle of the radiation of the corresponding string segment. We must caution that the existence of cosmic string is only speculative.

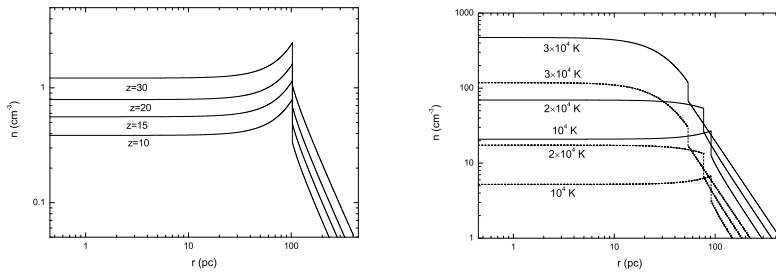


Fig. 12 *Left panel* Minihalo circumburst density. Shown is the hydrogen number density as a function of distance from the central Pop III star at the moment of its death. Typical circumburst densities are $\sim 1 \text{ cm}^{-3}$. *Right panel* Atomic-cooling-halo circumburst density. The density profiles are calculated from the Shu solution. The case of photoheating from only a single Pop III star (*solid lines*), and that from a stellar cluster (*dotted lines*). (Adapted from Figures 1 and 2 in Wang et al. (2012).)

4 Probing the Pop III stars and High-Redshift IGM

4.1 Observational signature of Pop III GRBs

The first stars, also called Population III (Pop III) stars, are predicted to have formed in minihaloes with virial temperatures $T_{\text{vir}} \leq 10^4 \text{ K}$ at $z \geq 15$ (Tegmark et al. 1997; Yoshida et al. 2003; Bromm & Larson 2004). Numerical simulations show that Pop III stars forming in primordial minihaloes, were predominantly very massive stars with typical masses $M_* \geq 100 M_{\odot}$ (Bromm et al. 1999, 2002), for recent reviews, see (Bromm et al. 2009). They had likely played a crucial role in early universe evolution, including reionization, metal enrichment history. Some studies shows that some Pop III stars will end as GRBs, called Pop III GRBs (Heger et al. 2003; Bromm & Loeb 2006; Komissarov & Barkov 2010; Stacy et al. 2011), which will be brighter and more energetic than any GRB yet detected (Toma et al. 2011; Nagakura et al. 2011; Campisi et al. 2011; Mészáros & Rees 2010; Nakauchi et al. 2012). Direct observations of the Pop III stars have so far been out of reach. The properties of Pop III stars may be revealed by their remanents, Pop III GRBs.

In particular, the afterglow emission of Pop III GRBs depend on the circumburst density (Ciardi & Loeb 2000; Gou et al. 2004; Wang et al. 2012). In particular, the central minihalo environments just before a massive star die and a GRB bursts out can be understood as follows. The number of ionizing photons depends strongly on the central stellar mass, which is determined by a accretion flow onto the growing protostar (e.g., McKee & Tan 2008; Hosokawa et al. 2011; Stacy et al. 2012). Meanwhile the accretion is also affected by this radiation field. So the assembly of the Pop III stars and the development of an H II region around them proceed simultaneously, and affect each other. The shallow potential wells of minihalos are unable to maintain photo-ionized gas, so that the gas is effectively blown out of the minihalo. The resulting photo-evaporation has been studied (Alvarez et al. 2006; Abel et al. 2002; Greif et al. 2009).

The photoevaporation from minihalos can be described as the self-similar solution for a champagne flow (Shu et al. 2002). Assuming a $\rho \propto r^{-2}$ density profile,

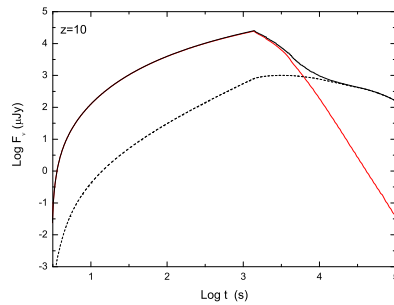


Fig. 13 Light curve at $\nu = 6.3 \times 10^{13}$ Hz (M band) of Pop III GRBs. The emission from the forward shock (*dashed line*), the reverse shock (*solid red line*), and their combination (*solid black line*) are shown. (Adapted from Figure 5 in Wang et al. (2012).)

the spherically symmetric continuity and Euler equations for isothermal gas can be described as follows:

$$[(v-x)^2 - 1] \frac{1}{\alpha} \frac{d\alpha}{dx} = \left[\alpha - \frac{2}{x}(x-v) \right] (x-v), \quad (27)$$

$$[(v-x)^2 - 1] \frac{dv}{dx} = \left[(x-v)\alpha - \frac{2}{x} \right] (x-v), \quad (28)$$

where $x = r/c_s t$, and $\rho(r, t) = \alpha(x)/4\pi G t^2 = m_{\text{H}} n(r)/X$ and $u(r, t) = c_s v(x)$ are the reduced density and velocity, respectively. c_s is the sound speed and $X = 0.75$ the hydrogen mass fraction. We set the typical lifetime of a massive Pop III star as $t = t_* \simeq 3 \times 10^6$ yr.

In the left panel of Figure 12, we show the density profiles at the end of the Pop III progenitor's life in the minihalo case. The circumstellar densities are nearly uniform at small radii. Such a flat density profile is markedly different from that created by stellar winds. But in the atomic cooling halo case, star formation and radiative feedback is not well understood (Johnson et al. 2009), such as the masses of stars, and stellar multiplicity (Clark et al. 2011). So we also use the formalism of the Shu solution as above. We assume that either one Pop III star or a small stellar cluster forms. The densities are shown in the right panel of Figure 12. Similar to the minihalo case, densities are nearly constant at small radii, but overall values are much higher, which is due to the deep potential wells, so that photoheated gas can easily be retained. Typical circumburst densities are $n \sim 100 \text{ cm}^{-3}$. Pop III GRBs originating in atomic cooling halos may be extremely bright.

The typical parameters of the afterglow emission are adopted, $\Gamma_0 = 300$, $E_{\text{iso}} = 10^{53}$ erg, $\Delta_0 = 10^{12}$ cm, $\epsilon_e = 0.3$, $\epsilon_B = 0.1$, and $p = 2.5$. As an example, in Figure 13, the M-band ($\nu = 6.3 \times 10^{13}$ Hz) light curve is shown. Figure 14 gives the observed flux at $\nu = 1.36 \times 10^{14}$ Hz as a function of redshift in the minihalo case. The lines with filled dots, black triangles and open dots correspond to an observed time of 6 minutes, 1 hour, and 1 day respectively. The straight line marks the K-band sensitivity for the near-infrared spectrograph (NIRSpec) on James Webb Space Telescope (Gardner et al. 2006). The high-redshift cut-off is

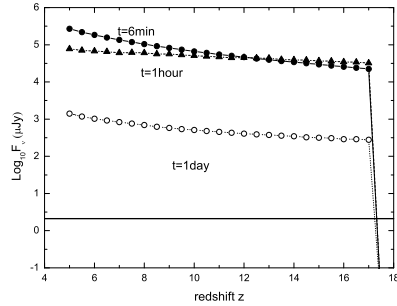


Fig. 14 Observed flux at $\nu = 1.36 \times 10^{14}$ Hz (K band) as a function of redshift at different observed times, as labelled. The K-band sensitivity of the NIRSpect instrument on board the *JWST* is shown as a horizontal line. The sharp cut-off at $z \simeq 17$ is due to Ly α absorption in the IGM. (Adapted from Figure 6 in Wang et al. (2012).)

due to the Ly α absorption. The flux will be completely absorbed by the intervening neutral IGM. At these frequencies, the flux of afterglow is weakly dependent on redshift of GRB. There are two reasons. First, the time dilation effect implies that the high redshift means the earlier emission times, where the afterglow are much brighter (Ciardi & Loeb 2000; Bromm & Loeb 2007). Second, circumburst densities of GRBs modestly increase with redshift.

4.2 Metal enrichment history

The metal enrichment history has several important influences for cosmic structure formation. For example, the metal injection change the mode of star formation (Bromm et al. 2001; Schneider et al. 2002). The transition between Pop III star formation and “normal” (Pop I/II) star formation has important implications, e.g., the expected GRB redshift distribution (Bromm et al. 2002), reionization (Wyithe & Loeb 2003), and the chemical abundance patterns of stars. So it is important to map the topology of pre-galactic metal enrichment. Ten or thirty meter-class telescopes have been proposed to measure the $z > 6$ IGM metallicity with the GRB afterglow (Oh 2002). Meanwhile, the relative gas column density from metal absorption lines can reflect the enrichment history (Hartmann 2008; Wang et al. 2012).

Absorption processes and absorption lines imprinted on the spectra of GRBs or quasars are the main sources of information about the chemical and physical properties of high-redshift universe. But the bright QSO number is very low at $z > 6$ (Fan et al. 2006). Meanwhile, there are several high-redshift GRBs: GRB 050904 at $z = 6.29$, GRB 080913 at $z = 6.7$, GRB 090423 at $z = 8.3$ and GRB 090429B at $z = 9.4$. The progenitors of long GRBs are thought to be massive stars, so the number of high-redshift GRBs does not decrease significantly. The density, temperature, kinematics and chemical abundances can be extracted from absorption lines (Oh 2002; Furlanetto & Loeb 2003). For instance, (Kawai et al. 2006) have identified several metal absorption lines in the afterglow spectrum

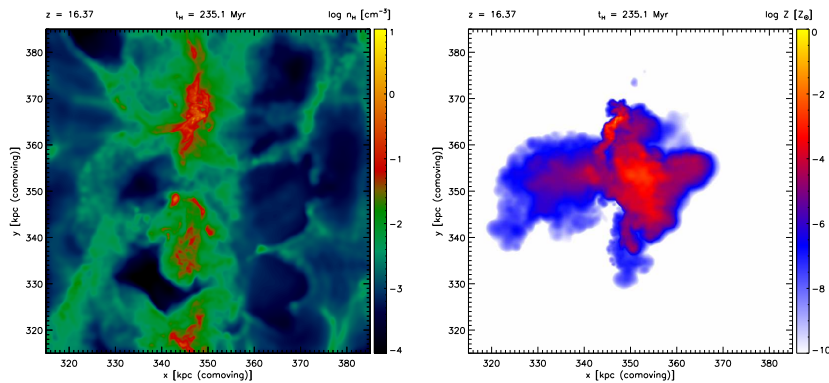


Fig. 15 Possible explosion sites for high-redshift GRBs. Shown are the hydrogen number density (left panel) and metallicity contours (right panel) averaged along the line of sight at $z \sim 16.37$, when the first galaxy forms. The topology of metal enrichment is highly inhomogeneous. (Adapted from Figure 3 in Wang et al. (2012).)

of GRB 050904 and found that this GRB occur in metal-enriched regions. Two absorption lines have been observed in the spectrum of GRB 090423 at $z = 8.2$ (Salvaterra et al. 2009). These lines are due mainly to absorption metal elements in low ionization stages.

Wang et al. (2012) studied the ability of metal absorption lines in the spectra of Pop III GRBs to probe the pre-galactic metal enrichment. The first galaxy simulation carried out by (Greif et al. 2010) was used. The simulation allowed one Pop III progenitor star to explode as an energetic supernova, then the IGM was polluted by the ejected metals. The simulation box size is 1 Mpc (comoving), and is initialized at $z = 99$ according to the Λ CDM model with parameters: $\Omega_m = 1 - \Omega_\Lambda = 0.3$, $\Omega_b = 0.04$, $h = H_0 / (100 \text{ km s}^{-1} \text{ Mpc}^{-1}) = 0.7$, spectral index $n_s = 1.0$, and normalization $\sigma_8 = 0.9$ (Spergel et al. 2003).

In Figure 18, the hydrogen number density and metallicity averaged along the line of sight are shown within the central $\simeq 100$ kpc closer to the virialization of the first galaxy at $z = 16.4$. The distribution of metals produced by the first SN explosion is highly inhomogeneous, and the metallicity can reach up to $Z \sim 10^{-2.5} Z_\odot$, which is already larger than the critical metallicity, $Z_{\text{crit}} \leq 10^{-4} Z_\odot$. Therefore, both Pop III and Pop I/II stars will form during the assembly of the first galaxies (Johnson et al. 2008; Maio et al. 2010), so simultaneous occurrence of Pop III and normal GRBs at a given redshift (Bromm & Loeb 2006; de Souza et al. 2011). We consider a Pop III burst exploding in one of the (still metal-free) first galaxy progenitor minihalos at $z \simeq 16.4$.

For simplicity, we consider that prior to the GRB only one nearby SN exploded beforehand, dispersing its heavy elements into the pristine IGM. Two nucleosynthetic metal yields for Type II core-collapse SNe (Woosley & Weaver 1995), and for pair-instability supernovae (PISNe; Heger & Woosley 2002, 2010) are considered. Because the hydrogen is substantially neutral, metals will reside in states typical of C II, O I, Si II, and Fe II, because high-energy photons able to further ionize these elements will be absorbed by H I (Furlanetto & Loeb 2003).

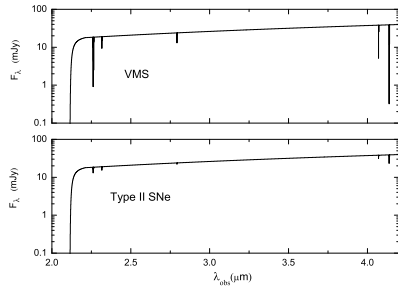


Fig. 16 Pop III GRB spectrum observed at the reverse shock crossing time $t_{\oplus} = 16.7 \times (1 + 16.4)$ s. Metal absorption lines are imprinted according to the Pop III SN event, PISN vs. core-collapse. The former originates from a very massive star (VMS) progenitor, whereas the latter from a less massive one. In each case, the cutoff at short wavelengths is due to Lyman- α scattering in the neutral IGM. (Adapted from Figure 10 in Wang et al. (2012).)

Figure 16 shows two spectra of afterglow at the reverse shock crossing time. Top panel is for the top-heavy (Very Massive Star) initial mass function (PISN case) and bottom for normal initial mass function (Type II SNe case). The cutoff is due to Lyman- α absorption in the IGM which is expected to be still completely neutral at $z > 10$. In the two cases, the metal lines are markedly different. The metal yields could be obtained from metal lines. So the initial mass function of Pop III stars can be derived from the metal absorption lines.

5 Using high resolution spectroscopy of GRBs to probe fundamental physics

5.1 Measuring the temperature of the cosmic microwave background radiation

The existence of the cosmic microwave background (CMB) radiation is a fundamental prediction of the hot Big-Bang theory. If gravitation is described by general relativity and electromagnetism by the Maxwell theory, then photons propagate along null geodesics and the CMB black-body temperature must follow the relation $T_{\text{CMB}}(z) = T_{\text{CMB}}(0) \times (1+z)^{-1-\beta}$, with $\beta=0$ and $T_{\text{CMB}}(0) = 2.725 \pm 0.002$ K for the temperature measured locally. This relation, which is a theoretical consequence of the adiabatic expansion of the Universe, needs to be verified by direct measurements. This has deeper theoretical implications as well (Uzan et al. 2004). A non-zero β would indicate either a violation of the hypothesis of local position invariance (and thus of the equivalence principle) or that the number of photons is not conserved with the constraint that the energy injection does not induce spectral distortion of the CMB. In the first case, this should be associated with a variation of the fundamental constants (see next Section). There are currently two methods to measure T_{CMB} at redshifts $z > 0$. The first one relies on the measurement of a small change in the spectral intensity of the CMB towards clusters of galaxies owing to inverse Compton scattering of photons by the hot intra-cluster gas: the so-called Sunyaev-Zeldovich (S-Z) effect. Although this technique per-

mits precise measurements $\Delta T \sim 0.3$ K (Luzzi et al. 2009; Hurier et al. 2014), the method is essentially limited to $z < 1$ because of the scarcity of known clusters at higher redshifts. The other technique uses the excitation of interstellar atomic or molecular species that have transition energies in the sub-millimetre range and can be excited by CMB photons. When the relative population of the different energy levels are in radiative equilibrium with the CMB radiation, the excitation temperature of the species equals that of the black-body radiation at that redshift. Therefore, the detection of these species in diffuse gas, where collisional excitation is negligible, provides one of the best thermometers for determining the black-body temperature of the CMB in the distant Universe (Bahcall & Wolf 1968; Molaro et al. 2002; Srianand et al. 2008).

One of the best thermometers is the molecule CO because it has a non-zero electromagnetic dipole which implies that in usual conditions of the *diffuse* interstellar medium (ISM), the excitation of the molecule is low (~ 5 K). Therefore at high redshift, the excitation is easily dominated by the CMB radiation. However, up to very recently, detection of the diffuse CO medium remained elusive and this is only very recently, thanks to the advent of large spectroscopic surveys of quasars that a dozen of such systems have been detected (Noterdaeme et al. 2010) resulting in the best constrain on β shown in Fig. 17.

Up to now only one CO detection has been reported in the spectrum of a GRB afterglow (Prochaska et al. 2009). This is unfortunately a case where the afterglow is highly obscured. However, due to the location of the GRB close to ISM of the host galaxy, the probability to detect diffuse molecular gas (and therefore to avoid very high extinction) is much higher in GRBs than in quasars. With the increased number of GRB detections at high redshift ($z > 3$) there is no doubt that such observations will be performed in the future. It is adamant however that to be successful, a high resolution spectrograph must be available at the extremely large telescopes to be built in the near future.

5.2 Testing variations of fundamental constants of physics

Metal lines of absorption systems due to intervening galaxies along the line of sight towards distant sources provide insight into the atomic structure at the cosmic time and location of the intervening object. All atomic transitions depend on the fine-structure constant, offering a way to probe possible variations in its value in space and time. These absorption lines are readily observed in the spectra of GRB afterglows and could be used to probe these possible variations.

A first analysis using the multi multiplet method on quasar absorption spectra obtained at the Keck telescope revealed hints that in the early universe the fine structure constant was smaller than today by ~ 6 parts per million (ppm; Murphy et al. 2003). However, the analysis of smaller data sets obtained from the Very Large Telescope (VLT) in Chile by other groups did not confirm the variation (Srianand et al. 2004, 2007). A recent analysis has been performed on a new sample built up by merging 141 measurements from Keck with 154 measurements from VLT (King et al. 2012). The merged sample confirms the results by Srianand et al. (2007) but indicates a spatial variation across the sky at the 4.1σ level with amplitude ~ 10 ppm. Since the Keck telescope in Hawaii is at a latitude of 20 degree North, and the VLT in Chile is at latitude of 25 degrees South,

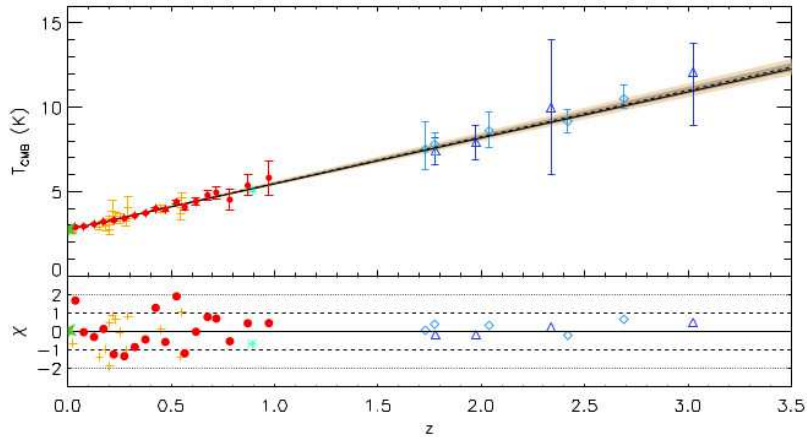


Fig. 17 *Top panel:* T_{CMB} as a function of redshift. The red filled circles represent SZ measurements in clusters by the Planck mission (Hurier et al. 2014). Blue diamonds show the measurements from CO absorption lines. The solid black line presents the standard evolution for T_{CMB} and the dashed black line represents the best-fitting model combining all the measurements. The 1 and 2σ envelopes are displayed as shaded dark and light-gray regions. *Bottom panel:* deviation from the standard evolution in units of standard deviation. The dashed and dotted black lines correspond to the 1 and 2σ levels. Figure is from Hurier et al. (2014) Note that only one high precision measurement using CO at high redshift could yield much stronger constraint on β .

the two subsamples survey relatively different hemispheres, and the study of the merged sample provides a much more complete sky coverage. Remarkably, the two sets of measurements are consistent along the region of the sky covered by the two telescopes. So far, this spatial variation has not been confirmed by other groups (e.g. Agafonova et al. 2011) but the lines-of-sight used by these groups fall into a region with minimal reported variation (see however Srikanth et al. 2012). One important weakness in the evidence for variations in α is that it derives mostly from archival Keck and VLT spectra.

A VLT/UVES large program has been dedicated to reach the ultimate precision and therefore track systematics. For this, twelve quasar lines-of-sight have been observed at the highest spectral resolution ($R \sim 60,000$) and highest SNR (> 100) possible. Along each line-of-sight there is at least one absorber in which we expect a precision approaching 2 ppm on the variation of α based on the variety of metal-line transitions available and the shape/structure of their absorption profiles (see Molaro et al. 2013). Some of the lines-of-sight are also dedicated to constraining the variations of μ , the electron-to-proton mass ratio (Rahmani et al. 2013).

GRB afterglows, if well selected, can be unique targets in this field after the advent of extremely large telescopes (TMT and ELT) since GRB afterglows can be very bright even at high redshift and yield spectra of the highest SNR; and the probability that the line-of-sight intersects a diffuse molecular cloud is much higher in the case of GRBs compared to QSOs. However, a fast response mode on a high resolution spectrograph has to be available (e.g. Vreeswijk et al. 2007) in order to collect a high SNR spectrum. It will also be important to follow a well defined procedure for wavelength calibration.

6 Using high energetic photons of GRBs to test fundamental physics

6.1 Constraining Lorentz invariance violation

Lorentz invariance is a famous postulate of Einstein's special relativity, which indicates that the relevant physics laws of a non-accelerated physical system are not affected when this system undergoes Lorentz transformation. However, many Quantum Gravity (QG) theories have suggested that quantum fluctuations in the space-time would make it appears discontinuous and chaotic, namely the foamy structure (Amelino-Camelia et al. 1997). And the propagation of light through the space-time with the foamy structure would show a non-trivial dispersion relation in vacuum (Amelino-Camelia et al. 1998), which could leads to the violation of Lorentz invariance. Constraining the Lorentz invariance violation (LIV) effect has been thought as an effective method to test the accuracy of QG theories, such as loop quantum gravity (Gambini & Pullin 1999; Alfaro et al. 2002), string theory (Kostelecký & Samuel 1989), double special relativity (Amelino-Camelia & Ahluwalia 2002), and so on. Since it is generally expected for QG to manifest itself fully at the Planck scale, the Planck energy scale ($E_{\text{QG}} \approx E_{\text{Pl}} = \sqrt{\hbar c^5/G} \simeq 1.22 \times 10^{19}$) being a natural one at which Lorentz invariance is predicted to be broken (see, e.g., Amelino-Camelia 2013, and references therein).

Due to the LIV effect, the speed for the propagation of photons could become energy-dependent, instead of a constant speed of light in vacuum (see Amelino-Camelia et al. 1998; Ellis & Mavromatos 2013). Normally, the modified dispersion relation of photons can be approximatively described as the leading term of the Taylor expansion (see Ellis et al. 2003; Jacob & Piran 2008)

$$E^2 \simeq p^2 c^2 \left[1 - s_n \left(\frac{pc}{E_{\text{QG},n}} \right)^n \right], \quad (29)$$

where the n-th order expansion of leading term corresponds to linear (n=1) or quadratic (n=2), E_{QG} denotes the QG energy scale, and $s_n = \pm 1$ represents the sign of the LIV correction. If $s_n = -1$ ($s_n = +1$), the low energy photons travel slower (faster) than the high energy photons. The speed of light derived from Equation (29) is

$$v = \frac{\partial E}{\partial p} \approx c \left[1 - s_n \frac{n+1}{2} \left(\frac{E}{E_{\text{QG},n}} \right)^n \right]. \quad (30)$$

Because of the energy dependence of the light speed, two photons with different energies emitted simultaneously from the source will reach us with a time delay Δt . For a cosmic source, the cosmological expansion should be taken into account when calculating the LIV induced time delay (Ellis et al. 2008; Jacob & Piran 2008; Zhang & Ma 2015)

$$\Delta t_{\text{LIV}} = t_h - t_l = s_n \frac{1+n}{2H_0} \frac{E_h^n - E_l^n}{E_{\text{QG},n}^n} \int_0^z \frac{(1+z')^n dz'}{\sqrt{\Omega_m(1+z')^3 + \Omega_\Lambda}}, \quad (31)$$

where t_h and t_l correspond to the arrival times of the high energy photon and the low energy one, with E_h and E_l ($E_h > E_l$) being the photon energies.

Since photons with different energies will arrive on earth at different time, GRBs with detected high energetic photons and measured redshifts have been proposed to test the LIV effect (see, e.g., Amelino-Camelia et al. 1998; Ellis et al.

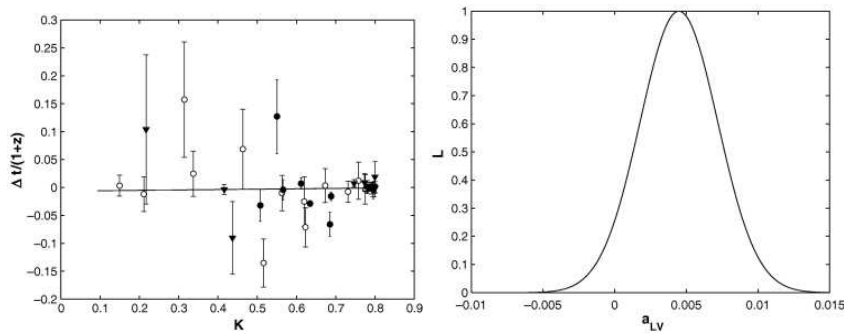


Fig. 18 Left panel: the observed spectral time-delays between the arrival times of pairs of genuine high-intensity sharp features detected in the light curves of the full set of 35 GRBs with measured redshifts observed by BATSE (closed circles), HETE (open circles) and SWIFT (triangles). Right panel: the likelihood function for the slope parameter. (Adapted from Figures 1 and 2 in Ellis et al. (2008).)

2003, 2006, 2008; Jacob & Piran 2008; Abdo et al. 2009b,a; Vasileiou et al. 2013; Zhang & Ma 2015). The first attempt that take the advantage of cosmological distances compared the arrival time of different energetic photons from GRB to constrain the LIV effect was presented in Amelino-Camelia et al. (1998). Ellis et al. (2003, 2006, 2008) developed a method to measure LIV by analyzing a large sample of GRBs with known redshifts. This method has the advantage that it can precisely extract the observed time lag from the GRB light curves in different energy bands. Taking into account the unknown intrinsic time lags b_{sf} , the observed time delays should have two contributions $\Delta t_{obs} = \Delta t_{LV} + b_{sf}(1+z)$ (Ellis et al. 2006). A simple linear fitting function can be written as

$$\frac{\Delta t_{obs}}{1+z} = a_{LV}K + b_{sf}, \quad (32)$$

where $K = (1+z)^{-1} \int_0^z dz' (1+z') / \sqrt{\Omega_m(1+z')^3 + \Omega_\Lambda}$ is a function of redshift and the slope $a_{LV} = \Delta E / (H_0 E_{QG})$ is related to the scale of Lorentz violation. Note that the linear term ($n=1$) is considered here. The result of a linear fit to the observed time delays extracted from 35 GRB light curves is presented in the left panel of Figure 18. The best fit corresponds to $\frac{\Delta t_{obs}}{1+z} = (0.0068 \pm 0.0067)K - (0.0065 \pm 0.0046)$ and the likelihood function for the slope a_{LV} is shown in the right panel of Figure 18. The 95% confidence-level lower limit on the QG energy scale derived from a_{LV} is $E_{QG} \geq 1.4 \times 10^{16}$ GeV (Ellis et al. 2008).

However, there is a limitation of Ellis et al. treatment. They extracted spectral time-lags in the light curves recorded in the MeV energy band relative to those in the keV energy band. The value of the energy band plays an important role in constraining LIV, a higher energy band leading to better constraints on LIV. Therefore, it is necessary to consider using the GeV lags to constrain LIV. Abdo et al. (2009b) used the highest energy (13.2 GeV) photon of GRB 080916C to study the LIV effect, which was detected 16.5 s after the trigger time.¹ Compared with previous estimates, their limit on the linear term ($E_{QG,1}$) of 1.3×10^{18}

¹ Since the energies of photons arrived at the trigger time (~ 100 keV) are several orders of magnitude lower than those of high energy photons (\sim GeV), $E_h^n - E_l^n$ in Equation (31) can be approximated as E_h^n .

GeV represented an improvement of one order of magnitude. But, it is still one order of magnitude below the Planck energy scale E_{Pl} . With an observed time delay ~ 0.86 s of GRB 090510 (i.e., the time lag between the trigger time and the arrival time of 31 GeV photon), Abdo et al. (2009a) set the most stringent limits on both the linear and quadratic term up to now. The limits set are $E_{\text{QG},1} > 9.1 \times 10^{19}$ GeV $> 1.2E_{\text{Pl}}$ and $E_{\text{QG},2} > 1.3 \times 10^{11}$ GeV. We can see that the linear (n=1) LIV can be excluded by GRB 090510.

6.2 Testing Einstein's Equivalence Principle

The Einstein Equivalence Principle (EEP) is the heart and soul of general relativity and other gravitational theories, which states that the trajectory of any uncharged “test” body is independent of its internal structure and composition. An alternative statement of the EEP is that spacetime is given a symmetric metric and uncharged test bodies follow geodesics of that metric. A lot of methods have been performed to quantify the possible violations of the EEP. Among the most famous are the Eötvös-type experiments, which compare the accelerations of two laboratory-sized bodies made of different composition in a gravitational field (see, e.g., Will 2014, and references therein). If the EEP is violated, the accelerations of these two bodies will be different. The validity of the EEP can be well tested by the comparison of laboratory-sized bodies in a Newtonian context. Nevertheless, Newtonian dynamics is inappropriate for describing particles’ (like photons or neutrinos) motion in a gravitational field. In order to measure the accuracy of the EEP with particles, the parameterized post-Newtonian (PPN) formalism has been developed for precisely describing their motion. Most metric theories of gravity satisfying the EEP are contained by the PPN formalism, and each theory is specified by the numerical values of some coefficients (PPN parameters), which have been well reviewed by Will (2006, 2014). The accuracy of the EEP can therefore be tested through the numerical values of PPN parameters.

For instance, Shapiro (1964) has suggested that the time interval for photons or neutrinos to pass through a given distance is longer within an external gravitational potential $U(r)$, the so-called Shapiro time delay, which is given by

$$\delta t = -\frac{1+\gamma}{c^3} \int_{r_e}^{r_o} U(r) dr, \quad (33)$$

where r_e and r_o are locations of source and observation, the PPN parameter γ accounts for how much space-curvature is produced by unit rest mass. General relativity predict that the value of γ should be unity (i.e., $\gamma = 1$), but not all gravity theories predict the same values for γ . There are many ways in which one can test general relativity by measuring the value of γ . Measurements of the parameter γ have reached high precision with the results of solar-system experiments, including the deflection of light and the time delay of light. The most stringent limits on the γ value from the light deflection near the sun is based on the very long baseline radio interferometry measurement, with a result $\gamma - 1 = (-0.8 \pm 1.2) \times 10^{-4}$ (Lambert & Le Poncin-Lafitte 2009, 2011). With the travel time delay of a radar signal of the Cassini spacecraft, Bertotti et al. (2003) set the most precise limit on the value of γ , i.e., $\gamma - 1 = (2.1 \pm 2.3) \times 10^{-5}$. These results showed that γ is very close to 1, which is consistent with the expectation of general relativity.

However, it is important to note that all gravity theories satisfying the EEP also predict $\gamma_1 = \gamma_2 \equiv \gamma$, where the subscripts represent two different test particles. To test the EEP in general relativity, therefore, the issue is not only whether the value of γ is very nearly 1, but also whether it is the same for different types of particles, or for the same type of particle with different energies. Krauss & Tremaine (1988) and Longo (1988) suggested that the small arrival time delay of the photon and neutrino emitted from supernova 1987A in the Large Magellanic Cloud provides a new precision test of the EEP. By analysing the arrival time delay between the photons (eV) and neutrinos (MeV) from supernova 1987A, Longo (1988) obtained a strong limit on the differences of γ to the level of 0.34%. In addition, using the time delay for two neutrinos with different energies, Longo (1988) set a more precise limit on γ differences, yielding $[\gamma(40 \text{ MeV}) - \gamma(7.5 \text{ MeV})] \leq 1.6 \times 10^{-6}$. Besides the extragalactic source (supernova 1987A), the nearly simultaneous arrival of photons with different energies from cosmic transients, such as GRBs, have also been applied to test the EEP (Sivaram 1999; Gao et al. 2015).

For a cosmic source, the observed time delays between correlated photons should have four contributions (Gao et al. 2015):

$$\Delta t_{\text{obs}} = \Delta t_{\text{int}} + \Delta t_{\text{LIV}} + \Delta t_{\text{spe}} + \Delta t_{\text{gra}}, \quad (34)$$

where Δt_{int} represents the unknown intrinsic time lag, Δt_{LIV} is the LIV induced time delay, and Δt_{spe} denotes the potential time delay caused by the non-zero mass of photons in special relativity. With Equation (33), the time delay (Δt_{gra}) of two photons with energy E_1 and E_2 , due to the external gravitational potential $U(r)$, which can be written down as

$$\Delta t_{\text{gra}} = \frac{\gamma_1 - \gamma_2}{c^3} \int_{r_o}^{r_e} U(r) dr. \quad (35)$$

Since both Δt_{LIV} and Δt_{spe} are negligible for the purposes of testing the EEP, they can be ignored in the analysis (see Gao et al. 2015, for more explanations). With the assumption that $\Delta t_{\text{int}} > 0$, one can derive

$$\Delta t_{\text{obs}} > \frac{\gamma_1 - \gamma_2}{c^3} \int_{r_o}^{r_e} U(r) dr. \quad (36)$$

Generally speaking, $U(r)$ should have three contributions: the gravitational potential of our galaxy $U_{\text{MW}}(r)$, the intergalactic potential $U_{\text{IG}}(r)$ between our galaxy and the transient host galaxy, and the gravitational potential of the transient host galaxy $U_{\text{host}}(r)$. Unfortunately, we know nothing about the potential functions for $U_{\text{IG}}(r)$ and $U_{\text{host}}(r)$, but we stand a good chance of considering the combination of these two terms is much larger than the potential of $U_{\text{MW}}(r)$. Hence, it would be reasonable to derive

$$\Delta t_{\text{obs}} > \frac{\gamma_1 - \gamma_2}{c^3} \int_{r_o}^{r_e} U_{\text{MW}}(r) dr. \quad (37)$$

If we adopt the Keplerian potential $U_{\text{MW}}(r) = -GM/r$ for our galaxy, then we have

$$\gamma_1 - \gamma_2 < \Delta t_{\text{obs}} \left(\frac{GM_{\text{MW}}}{c^3} \right)^{-1} \ln^{-1} \left(\frac{d}{b} \right), \quad (38)$$

where $M_{\text{MW}} \simeq 6 \times 10^{11} M_{\odot}$ represents the mass of our galaxy (McMillan 2011; Kafle et al. 2012), d is the distance from the transient source to the observer, and b denotes the impact parameters of the light rays relative to our galaxy center. Assuming that the cosmic transient source located in the direction (R.A.= β_S , Dec.= δ_S), the impact parameter b can be calculated by the expression

$$b = r_G \sqrt{1 - (\sin \delta_S \sin \delta_G + \cos \delta_S \cos \delta_G \cos (\beta_S - \beta_G))^2}, \quad (39)$$

where $r_G = 8.3$ kpc is the distance from the Sun to our galaxy center, and the coordinates (J2000) of our galaxy center correspond to $\beta_G = 17^{\text{h}}45^{\text{m}}40.04^{\text{s}}$ and $\delta_G = -29^{\circ}00'28.1''$ (Gillessen et al. 2009).

With the assumption that the observed time delays for photons with different energies are caused dominantly by the gravitational potential of our galaxy, for the GeV and MeV photons of GRB 090510 Gao et al. (2015) set a severe limit of $\gamma_{\text{GeV}} - \gamma_{\text{MeV}} \leq 2 \times 10^{-8}$; and for the optical and MeV photons from GRB 080319B they obtained $\gamma_{\text{eV}} - \gamma_{\text{MeV}} \leq 1.2 \times 10^{-7}$. Comparing these results with the limits of supernovae 1987 shows that GRBs can increase the accuracy level of the EEP constraints by at least one order of magnitude, to $\sim 10^{-7}$, while expanding the tested EEP energy range to the MeV-eV and GeV-MeV range. Sivaram (1999) also derived the same upper limit on the EEP of 4×10^{-7} for gamma-ray and optical photons from GRB 990123, but his result was restricted to the MeV and eV energy bands.

7 Summary and future prospect

GRBs are observed throughout the whole electromagnetic spectrum, from radio waves to γ -rays, which have been observed in distant universe. Recently, GRBs have attracted a lot of attention as promising standardizable candles to construct the Hubble diagram to high redshift, as complementarity to other cosmological probes, such as SNe Ia, CMB and BAO. However, a lot of work is needed to be sure that GRBs can hold this promise in future. The most important thing is to search for a correlation similar to that used to standardize SNe Ia. In order to obtain the correlation, the classification of GRBs may be crucial. We must remind that only SNe Ia are standard candles among all SNe. The classical classification method is based on the prompt emission properties (duration, hardness, and spectral lag). The physics of prompt emission are not fully understood (Zhang 2014), and some new clues from other objects are found (Wang & Dai 2013; Wang et al. 2014). But observations of some GRBs are challenging the standard classification (Zhang 2006; Zhang et al. 2009; Lü et al. 2010). So more physical nature of GRBs is needed (Zhang et al. 2009). The circularity problem could be partially solved by analyzing a sample of GRBs within a small redshift bin (Ghirlanda et al. 2006; Liang & Zhang 2006).

In order to measure high-redshift SFR from GRBs, the relation between long GRB rate and SFR must be known. Besides, theoretical models of the SFR have several free parameters, such as the efficiency of star formation and the chemical feedback strength. From the theoretical SFR, the predicted GRB redshift distribution can be derived. So one can use the GRB redshift distribution observed by

Swift (or future missions such as SVOM and EXIST), to calibrate the free parameters. More GRB red damping wing with low HI column density are required to study properties of IGM.

Metal absorption lines in the GRB afterglow spectrum, giving rise to EWs of a few tens of Å, which may allow us to distinguish whether the first heavy elements were produced in a Pop III star died as a PISN or a core-collapse SN. To this extent, the spectrum needs to be obtained sufficiently early, within the first few hours after the trigger. Upcoming JWST would detect much more high-redshift GRBs (properly Pop III GRBs) with high resolution NIR spectra including metal absorption lines, which allow one to measure the cosmic metallicity evolution.

In the future, the French-Chinese satellite Space-based multi-band astronomical Variable Objects Monitor (SVOM) and JWST, have been optimized to increase the number of GRB and the synergy with the ground-based facilities. There are a combination of multi-wavelength detectors on board of SVOM (Paul et al. 2011). ECLAIRS wide-field camera will detect GRBs in the energy range of 4-150 keV. The spectral information of prompt emission will be measured by Gamma-Ray Monitor (GRM). The afterglow can be obtained by the Micro channel X-ray Telescope (MXT; 0.3-10 keV) and the Visible Telescope (VT; 400-900nm). SVOM can detect about 80 GRBs per year, and more than 50% of GRBs have redshift measurement (Petitjean & Vergani 2011). JWST is a large, infrared-optimized space telescope with 6.6 m diameter aperture. It has four scientific instruments: a Near-IR Camera (NIRCam), a Near-IR Spectrograph (NIRSpec), a near-IR Tunable Filter Imager (TFI), and a Mid-IR Instrument (MIRI) (Gardner et al. 2006). But the direct detection of a single Pop III star is not feasible even for JWST, i.e., the AB magnitude of a $M = 1000M_{\odot}$ star is only 36 at $z \sim 30$. Meanwhile, the Pop III GRBs can be detectable by JWST (Wang et al. 2012; Mesler et al. 2014; Macpherson et al. 2013). This will boost the amount of information available to tackle the important issues revealed by this exciting field of research.

Because of the much larger detector area and higher sensitivity, the Water Cerenkov Detector Array (WCDA) of LHAASO will has the ability to detect much more high-energy photons from GRBs and high quality high-energy light curves will be possible, making it easy to extract the observed time delays from the light curves with different energy bands. We can expect that the high energy GRB observations provided by LHAASO/WCDA will set much more competitive limits on fundamental physics.

Acknowledgements This work is supported by the National Basic Research Program (“973” Program) of China (grants 2014CB845800 and 2013CB83490), the National Natural Science Foundation of China (grants 11422325, 11373022, 11033002, 11322328, and 11433009), the Excellent Youth Foundation of Jiangsu Province (BK20140016), and the Program for New Century Excellent Talents in University (grant No. NCET-13-0279). X. F. W. was also partially supported by the One-Hundred-Talent Program, the Youth Innovation Promotion Association (2011231), and the Strategic Priority Research Program “The Emergence of Cosmological Structure” (grant No. XDB09000000) of the Chinese Academy of Sciences.

References

Abdo, A. A., Ackermann, M., Ajello, M., Asano, K., Atwood, W. B., Axelsson, M., Baldini, L., Ballet, J., Barbiellini, G., Baring, M. G., & et al. 2009a, *Natur.*, 462, 331

- Abdo, A. A., Ackermann, M., Arimoto, M., Asano, K., Atwood, W. B., Axelsson, M., Baldini, L., Ballet, J., Band, D. L., Barbiellini, G., & et al. 2009b, *Science*, 323, 1688
- Abel, T., Bryan, G. L., & Norman, M. L. 2002, *Science*, 295, 93
- Agafonova, I. I., Molaro, P., Levshakov, S. A., & Hou, J. L. 2011, *Astron. Astrophys.*, 529, A28
- Alfaro, J., Morales-Técotl, H. A., & Urrutia, L. F. 2002, *Phys. Rev. D*, 65, 103509
- Allen, S. W., Schmidt, R. W., Ebeling, H., Fabian, A. C., & van Speybroeck, L. 2004, *Mon. Not. Roy. Astron. Soc.*, 353, 457
- Alvarez, M. A., Bromm, V., & Shapiro, P. R. 2006, *Astrophys. J.*, 639, 621
- Amati, L. 2006, *Mon. Not. Roy. Astron. Soc.*, 372, 233
- Amati, L., & Della Valle, M. 2013, *International Journal of Modern Physics D*, 22, 30028
- Amati, L., Frontera, F., Tavani, M., in't Zand, J. J. M., Antonelli, A., Costa, E., Feroci, M., Guidorzi, C., Heise, J., Masetti, N., Montanari, E., Nicastrò, L., Palazzi, E., Pian, E., Piro, L., & Soffitta, P. 2002, *Astron. Astrophys.*, 390, 81
- Amati, L., Guidorzi, C., Frontera, F., Della Valle, M., Finelli, F., Landi, R., & Montanari, E. 2008, *Mon. Not. Roy. Astron. Soc.*, 391, 577
- Amelino-Camelia, G. 2013, *Living Reviews in Relativity*, 16, 5
- Amelino-Camelia, G., & Ahluwalia, D. V. 2002, *International Journal of Modern Physics D*, 11, 35
- Amelino-Camelia, G., Ellis, J., Mavromatos, N. E., & Nanopoulos, D. V. 1997, *International Journal of Modern Physics A*, 12, 607
- Amelino-Camelia, G., Ellis, J., Mavromatos, N. E., Nanopoulos, D. V., & Sarkar, S. 1998, *Natur.*, 393, 763
- Bahcall, J. N., & Wolf, R. A. 1968, *Astrophys. J.*, 152, 701
- Band, D., Matteson, J., Ford, L., Schaefer, B., Palmer, D., Teegarden, B., Cline, T., Briggs, M., Paciesas, W., Pendleton, G., Fishman, G., Kouveliotou, C., Meegan, C., Wilson, R., & Lestrade, P. 1993, *Astrophys. J.*, 413, 281
- Basilakos, S., & Perivolaropoulos, L. 2008, *Mon. Not. Roy. Astron. Soc.*, 391, 411
- Berger, E. 2014, *Annu. Rev. Astron. Astr.*, 52, 43
- Bertolami, O., & Silva, P. T. 2006, *Mon. Not. Roy. Astron. Soc.*, 365, 1149
- Bertotti, B., Iess, L., & Tortora, P. 2003, *Natur.*, 425, 374
- Bloom, J. S., Butler, N. R., & Perley, D. A. 2008, in *American Institute of Physics Conference Series*, Vol. 1000, American Institute of Physics Conference Series, ed. M. Galassi, D. Palmer, & E. Fenimore, 11–15
- Bloom, J. S., Frail, D. A., & Kulkarni, S. R. 2003, *Astrophys. J.*, 594, 674
- Bloom, J. S., Frail, D. A., & Sari, R. 2001, *Astron. J.*, 121, 2879
- Bouwens, R. J., Illingworth, G. D., Franx, M., Chary, R.-R., Meurer, G. R., Conselice, C. J., Ford, H., Giavalisco, M., & van Dokkum, P. 2009, *Astrophys. J.*, 705, 936
- Bouwens, R. J., Illingworth, G. D., Labbe, I., Oesch, P. A., Trenti, M., Carollo, C. M., van Dokkum, P. G., Franx, M., Stiavelli, M., González, V., Magee, D., & Bradley, L. 2011, *Natur.*, 469, 504
- Bromm, V., Coppi, P. S., & Larson, R. B. 1999, *Astrophys. J. Lett.*, 527, L5
- , 2002, *Astrophys. J.*, 564, 23
- Bromm, V., Ferrara, A., Coppi, P. S., & Larson, R. B. 2001, *Mon. Not. Roy. Astron. Soc.*, 328, 969
- Bromm, V., & Larson, R. B. 2004, *Annu. Rev. Astron. Astr.*, 42, 79
- Bromm, V., & Loeb, A. 2006, *Astrophys. J.*, 642, 382
- , 2007, *ArXiv e-prints*
- Bromm, V., Yoshida, N., Hernquist, L., & McKee, C. F. 2009, *Natur.*, 459, 49
- Campisi, M. A., Li, L.-X., & Jakobsson, P. 2010, *Mon. Not. Roy. Astron. Soc.*, 407, 1972
- Campisi, M. A., Maio, U., Salvaterra, R., & Ciardi, B. 2011, *Mon. Not. Roy. Astron. Soc.*, 416, 2760
- Cao, X.-F., Yu, Y.-W., Cheng, K. S., & Zheng, X.-P. 2011, *Mon. Not. Roy. Astron. Soc.*, 416, 2174
- Capozziello, S., & Izzo, L. 2008, *Astron. Astrophys.*, 490, 31
- Cardone, V. F., Capozziello, S., & Dainotti, M. G. 2009, *Mon. Not. Roy. Astron. Soc.*, 400, 775
- Cheng, K. S., Yu, Y.-W., & Harko, T. 2010, *Physical Review Letters*, 104, 241102
- Cheng, K. S., Yu, Y. W., & Harko, T. 2011, *Physical Review Letters*, 106, 259002
- Ciardi, B., & Loeb, A. 2000, *Astrophys. J.*, 540, 687

- Clark, P. C., Glover, S. C. O., Klessen, R. S., & Bromm, V. 2011, *Astrophys. J.*, 727, 110
- Cobb, B. E., Baily, C. D., van Dokkum, P. G., & Natarajan, P. 2006, *Astrophys. J. Lett.*, 645, L113
- Coward, D. 2007, *New Atron. Rev.*, 51, 539
- Dai, Z. G., Liang, E. W., & Xu, D. 2004, *Astrophys. J. Lett.*, 612, L101
- Dai, Z. G., & Wang, F. Y. 2007, *Advances in Space Research*, 40, 1244
- Daigne, F., Rossi, E. M., & Mochkovitch, R. 2006, *Mon. Not. Roy. Astron. Soc.*, 372, 1034
- Davé, R. 2008, *Mon. Not. Roy. Astron. Soc.*, 385, 147
- de Souza, R. S., Yoshida, N., & Ioka, K. 2011, *Astron. Astrophys.*, 533, A32
- Demianski, M., & Piedipalumbo, E. 2011, *Mon. Not. Roy. Astron. Soc.*, 415, 3580
- Demianski, M., Piedipalumbo, E., & Rubano, C. 2011, *Mon. Not. Roy. Astron. Soc.*, 411, 1213
- Di Girolamo, T., Catena, R., Vietri, M., & Di Sciascio, G. 2005, *J. Cosmol. Astropart. P.*, 4, 8
- Efron, B., & Petrosian, V. 1992, *Astrophys. J.*, 399, 345
- Eisenstein, D. J., Zehavi, I., Hogg, D. W., Scoccimarro, R., Blanton, M. R., Nichol, R. C., Scranton, R., Seo, H.-J., Tegmark, M., Zheng, Z., Anderson, S. F., Annis, J., Bahcall, N., Brinkmann, J., Burles, S., Castander, F. J., Connolly, A., Csabai, I., Doi, M., Fukugita, M., Frieman, J. A., Glazebrook, K., Gunn, J. E., Hendry, J. S., Hennessy, G., Ivezić, Z., Kent, S., Knapp, G. R., Lin, H., Loh, Y.-S., Lupton, R. H., Margon, B., McKay, T. A., Meiksin, A., Munn, J. A., Pope, A., Richmond, M. W., Schlegel, D., Schneider, D. P., Shimasaku, K., Stoughton, C., Strauss, M. A., SubbaRao, M., Szalay, A. S., Szapudi, I., Tucker, D. L., Yanny, B., & York, D. G. 2005, *Astrophys. J.*, 633, 560
- Elliott, J., Greiner, J., Khochfar, S., Schady, P., Johnson, J. L., & Rau, A. 2012, *Astron. Astrophys.*, 539, A113
- Ellis, J., & Mavromatos, N. E. 2013, *Astroparticle Physics*, 43, 50
- Ellis, J., Mavromatos, N. E., Nanopoulos, D. V., & Sakharov, A. S. 2003, *Astron. Astrophys.*, 402, 409
- Ellis, J., Mavromatos, N. E., Nanopoulos, D. V., Sakharov, A. S., & Sarkisyan, E. K. G. 2006, *Astroparticle Physics*, 25, 402
- 2008, *Astroparticle Physics*, 29, 158
- Fan, X., Carilli, C. L., & Keating, B. 2006, *Annu. Rev. Astron. Astr.*, 44, 415
- Fenimore, E. E., & Ramirez-Ruiz, E. 2000, *ArXiv Astrophysics e-prints*
- Firmani, C., Ghisellini, G., Avila-Reese, V., & Ghirlanda, G. 2006, *Mon. Not. Roy. Astron. Soc.*, 370, 185
- Firmani, C., Ghisellini, G., Ghirlanda, G., & Avila-Reese, V. 2005, *Mon. Not. Roy. Astron. Soc.*, 360, L1
- Frail, D. A., Kulkarni, S. R., Sari, R., Djorgovski, S. G., Bloom, J. S., Galama, T. J., Reichart, D. E., Berger, E., Harrison, F. A., Price, P. A., Yost, S. A., Diercks, A., Goodrich, R. W., & Chaffee, F. 2001, *Astrophys. J. Lett.*, 562, L55
- Fruchter, A. S., Levan, A. J., Strolger, L., Vreeswijk, P. M., Thorsett, S. E., Bersier, D., Burud, I., Castro Cerón, J. M., Castro-Tirado, A. J., Conselice, C., Dahlen, T., Ferguson, H. C., Fynbo, J. P. U., Garnavich, P. M., Gibbons, R. A., Gorosabel, J., Gull, T. R., Hjorth, J., Holland, S. T., Kouveliotou, C., Levay, Z., Livio, M., Metzger, M. R., Nugent, P. E., Petro, L., Pian, E., Rhoads, J. E., Riess, A. G., Sahu, K. C., Smette, A., Tanvir, N. R., Wijers, R. A. M. J., & Woosley, S. E. 2006, *Natur.*, 441, 463
- Furlanetto, S. R., & Loeb, A. 2003, *Astrophys. J.*, 588, 18
- Gal-Yam, A., Fox, D. B., Price, P. A., Ofek, E. O., Davis, M. R., Leonard, D. C., Soderberg, A. M., Schmidt, B. P., Lewis, K. M., Peterson, B. A., Kulkarni, S. R., Berger, E., Cenko, S. B., Sari, R., Sharon, K., Frail, D., Moon, D.-S., Brown, P. J., Cucchiara, A., Harrison, F., Piran, T., Persson, S. E., McCarthy, P. J., Penprase, B. E., Chevalier, R. A., & MacFadyen, A. I. 2006, *Natur.*, 444, 1053
- Gambini, R., & Pullin, J. 1999, *Phys. Rev. D*, 59, 124021
- Gao, H., Liang, N., & Zhu, Z.-H. 2012, *International Journal of Modern Physics D*, 21, 50016
- Gao, H., Wu, X.-F., & Mészáros, P. 2015, *Astrophys. J.*, 810, 121
- Gardner, J. P., Mather, J. C., Clampin, M., Doyon, R., Greenhouse, M. A., Hammel, H. B., Hutchings, J. B., Jakobsen, P., Lilly, S. J., Long, K. S., Lunine, J. I., McCaughrean, M. J., Mountain, M., Nella, J., Rieke, G. H., Rieke, M. J., Rix, H.-W., Smith, E. P., Sonneborn, G., Stiavelli, M., Stockman, H. S., Windhorst, R. A., & Wright, G. S. 2006, *Space Sci. Rev.*, 123, 485
- Gehrels, N. 1986, *Astrophys. J.*, 303, 336

- Gehrels, N., Chincarini, G., Giommi, P., Mason, K. O., Nousek, J. A., Wells, A. A., White, N. E., Barthelmy, S. D., Burrows, D. N., Cominsky, L. R., Hurley, K. C., Marshall, F. E., Mészáros, P., Roming, P. W. A., Angelini, L., Barbier, L. M., Belloni, T., Campana, S., Caraveo, P. A., Chester, M. M., Citterio, O., Cline, T. L., Cropper, M. S., Cummings, J. R., Dean, A. J., Feigelson, E. D., Fenimore, E. E., Frail, D. A., Fruchter, A. S., Garmire, G. P., Gendreau, K., Ghisellini, G., Greiner, J., Hill, J. E., Hunsberger, S. D., Krimm, H. A., Kulkarni, S. R., Kumar, P., Lebrun, F., Lloyd-Ronning, N. M., Markwardt, C. B., Mattson, B. J., Mushotzky, R. F., Norris, J. P., Osborne, J., Paczynski, B., Palmer, D. M., Park, H.-S., Parsons, A. M., Paul, J., Rees, M. J., Reynolds, C. S., Rhoads, J. E., Sasseen, T. P., Schaefer, B. E., Short, A. T., Smale, A. P., Smith, I. A., Stella, L., Tagliaferri, G., Takahashi, T., Tashiro, M., Townsley, L. K., Tueller, J., Turner, M. J. L., Vietri, M., Voges, W., Ward, M. J., Willingale, R., Zerbi, F. M., & Zhang, W. W. 2004, *Astrophys. J.*, 611, 1005
- Gehrels, N., Norris, J. P., Barthelmy, S. D., Granot, J., Kaneko, Y., Kouveliotou, C., Markwardt, C. B., Mészáros, P., Nakar, E., Nousek, J. A., O'Brien, P. T., Page, M., Palmer, D. M., Parsons, A. M., Roming, P. W. A., Sakamoto, T., Sarazin, C. L., Schady, P., Stamatikos, M., & Woosley, S. E. 2006, *Natur.*, 444, 1044
- Gehrels, N., Ramirez-Ruiz, E., & Fox, D. B. 2009, *Annu. Rev. Astron. Astr.*, 47, 567
- Ghirlanda, G. 2009, in *American Institute of Physics Conference Series*, Vol. 1111, American Institute of Physics Conference Series, ed. G. Giobbi, A. Tornambe, G. Raimondo, M. Limongi, L. A. Antonelli, N. Menci, & E. Brocato, 579–586
- Ghirlanda, G., Ghisellini, G., & Firmani, C. 2006, *New Journal of Physics*, 8, 123
- Ghirlanda, G., Ghisellini, G., & Lazzati, D. 2004a, *Astrophys. J.*, 616, 331
- Ghirlanda, G., Ghisellini, G., Lazzati, D., & Firmani, C. 2004b, *Astrophys. J. Lett.*, 613, L13
- Gillessen, S., Eisenhauer, F., Trippe, S., Alexander, T., Genzel, R., Martins, F., & Ott, T. 2009, *Astrophys. J.*, 692, 1075
- Gou, L. J., Mészáros, P., Abel, T., & Zhang, B. 2004, *Astrophys. J.*, 604, 508
- Graham, J. F., Fruchter, A. S., Kewley, L. J., Levesque, E. M., Levan, A. J., Tanvir, N. R., Reichart, D. E., & Nysewander, M. 2009, in *American Institute of Physics Conference Series*, Vol. 1133, American Institute of Physics Conference Series, ed. C. Meegan, C. Kouveliotou, & N. Gehrels, 269–272
- Greif, T. H., Glover, S. C. O., Bromm, V., & Klessen, R. S. 2010, *Astrophys. J.*, 716, 510
- Greif, T. H., Johnson, J. L., Klessen, R. S., & Bromm, V. 2009, *Mon. Not. Roy. Astron. Soc.*, 399, 639
- Guetta, D., & Piran, T. 2007, *J. Cosmol. Astropart. P.*, 7, 3
- Guetta, D., Piran, T., & Waxman, E. 2005, *Astrophys. J.*, 619, 412
- Hao, J.-M., & Yuan, Y.-F. 2013, *Astrophys. J.*, 772, 42
- Hartmann, D. H. 2008, *New Astron. Rev.*, 52, 450
- Heger, A., Fryer, C. L., Woosley, S. E., Langer, N., & Hartmann, D. H. 2003, *Astrophys. J.*, 591, 288
- Heger, A., & Woosley, S. E. 2002, *Astrophys. J.*, 567, 532
- . 2010, *Astrophys. J.*, 724, 341
- Hirschi, R., Meynet, G., & Maeder, A. 2005, *Astron. Astrophys.*, 443, 581
- Hjorth, J., Sollerman, J., Møller, P., Fynbo, J. P. U., Woosley, S. E., Kouveliotou, C., Tanvir, N. R., Greiner, J., Andersen, M. I., Castro-Tirado, A. J., Castro Cerón, J. M., Fruchter, A. S., Gorosabel, J., Jakobsson, P., Kaper, L., Klose, S., Masetti, N., Pedersen, H., Pedersen, K., Pian, E., Palazzi, E., Rhoads, J. E., Rol, E., van den Heuvel, E. P. J., Vreeswijk, P. M., Watson, D., & Wijers, R. A. M. J. 2003, *Natur.*, 423, 847
- Holz, D. E. 1998, *Astrophys. J. Lett.*, 506, L1
- Hopkins, A. M., & Beacom, J. F. 2006, *Astrophys. J.*, 651, 142
- Hosokawa, T., Omukai, K., Yoshida, N., & Yorke, H. W. 2011, *Science*, 334, 1250
- Hurier, G., Aghanim, N., Douspis, M., & Pointecouteau, E. 2014, *Astron. Astrophys.*, 561, A143
- Izzo, L., Muccino, M., Zaninoni, E., Amati, L., & Della Valle, M. 2015, *ArXiv e-prints*
- Jacob, U., & Piran, T. 2008, *J. Cosmol. Astropart. P.*, 1, 31
- Jimenez, R., & Piran, T. 2013, *Astrophys. J.*, 773, 126
- Jimenez, R., Verde, L., Treu, T., & Stern, D. 2003, *Astrophys. J.*, 593, 622
- Johnson, J. L., Greif, T. H., & Bromm, V. 2008, *Mon. Not. Roy. Astron. Soc.*, 388, 26
- Johnson, J. L., Greif, T. H., Bromm, V., Klessen, R. S., & Ippolito, J. 2009, *Mon. Not. Roy. Astron. Soc.*, 399, 37

- Jones, D. O., Rodney, S. A., Riess, A. G., Mobasher, B., Dahlen, T., McCully, C., Frederiksen, T. F., Casertano, S., Hjorth, J., Keeton, C. R., Koekemoer, A., Strolger, L.-G., Wiklund, T. G., Challis, P., Graur, O., Hayden, B., Patel, B., Weiner, B. J., Filippenko, A. V., Garnavich, P., Jha, S. W., Kirshner, R. P., Ferguson, H. C., Grogin, N. A., & Kocevski, D. 2013, *Astrophys. J.*, 768, 166
- Kafle, P. R., Sharma, S., Lewis, G. F., & Bland-Hawthorn, J. 2012, *Astrophys. J.*, 761, 98
- Kawai, N., Kosugi, G., Aoki, K., Yamada, T., Totani, T., Ohta, K., Iye, M., Hattori, T., Aoki, W., Furusawa, H., Hurley, K., Kawabata, K. S., Kobayashi, N., Komiyama, Y., Mizumoto, Y., Nomoto, K., Noumaru, J., Ogasawara, R., Sato, R., Sekiguchi, K., Shirasaki, Y., Suzuki, M., Takata, T., Tamagawa, T., Terada, H., Watanabe, J., Yatsu, Y., & Yoshida, A. 2006, *Natur.*, 440, 184
- King, J. A., Webb, J. K., Murphy, M. T., Flambaum, V. V., Carswell, R. F., Bainbridge, M. B., Wilczynska, M. R., & Koch, F. E. 2012, *Mon. Not. Roy. Astron. Soc.*, 422, 3370
- Kistler, M. D., Yüksel, H., Beacom, J. F., Hopkins, A. M., & Wyithe, J. S. B. 2009, *Astrophys. J. Lett.*, 705, L104
- Kistler, M. D., Yüksel, H., Beacom, J. F., & Stanek, K. Z. 2008, *Astrophys. J. Lett.*, 673, L119
- Kocevski, D., West, A. A., & Modjaz, M. 2009, *Astrophys. J.*, 702, 377
- Kodama, Y., Yonetoku, D., Murakami, T., Tanabe, S., Tsutsui, R., & Nakamura, T. 2008, *Mon. Not. Roy. Astron. Soc.*, 391, L1
- Komatsu, E., Smith, K. M., Dunkley, J., Bennett, C. L., Gold, B., Hinshaw, G., Jarosik, N., Larson, D., Nolte, M. R., Page, L., Spergel, D. N., Halpern, M., Hill, R. S., Kogut, A., Limon, M., Meyer, S. S., Odegard, N., Tucker, G. S., Weiland, J. L., Wollack, E., & Wright, E. L. 2011, *Astrophys. J. Suppl.*, 192, 18
- Komissarov, S. S., & Barkov, M. V. 2010, *Mon. Not. Roy. Astron. Soc.*, 402, L25
- Kostelecký, V. A., & Samuel, S. 1989, *Phys. Rev. D*, 39, 683
- Kouveliotou, C., Meegan, C. A., Fishman, G. J., Bhat, N. P., Briggs, M. S., Koshut, T. M., Paciasas, W. S., & Pendleton, G. N. 1993, *Astrophys. J. Lett.*, 413, L101
- Krauss, L. M., & Tremaine, S. 1988, *Physical Review Letters*, 60, 176
- Kudritzki, R.-P., & Puls, J. 2000, *Annu. Rev. Astron. Astr.*, 38, 613
- Kumar, P., & Zhang, B. 2015, *Phys. Rep.*, 561, 1
- Lamb, D. Q., & Reichart, D. E. 2000, *Astrophys. J.*, 536, 1
- Lambert, S. B., & Le Poncin-Lafitte, C. 2009, *Astron. Astrophys.*, 499, 331
- . 2011, *Astron. Astrophys.*, 529, A70
- Langer, N., & Norman, C. A. 2006, *Astrophys. J. Lett.*, 638, L63
- Le, T., & Dermer, C. D. 2007, *Astrophys. J.*, 661, 394
- Levesque, E. M. 2014, *Publ. Astron. Soc. Pac.*, 126, 1
- Levesque, E. M., Kewley, L. J., Berger, E., & Zahid, H. J. 2010, *Astron. J.*, 140, 1557
- Li, H., Xia, J.-Q., Liu, J., Zhao, G.-B., Fan, Z.-H., & Zhang, X. 2008, *Astrophys. J.*, 680, 92
- Li, L.-X. 2007, *Mon. Not. Roy. Astron. Soc.*, 379, L55
- . 2008, *Mon. Not. Roy. Astron. Soc.*, 388, 1487
- Liang, E., & Zhang, B. 2005, *Astrophys. J.*, 633, 611
- . 2006, *Mon. Not. Roy. Astron. Soc.*, 369, L37
- Liang, E., Zhang, B., Virgili, F., & Dai, Z. G. 2007, *Astrophys. J.*, 662, 1111
- Liang, N., Xiao, W. K., Liu, Y., & Zhang, S. N. 2008, *Astrophys. J.*, 685, 354
- Lin, H.-N., Li, X., Wang, S., & Chang, Z. 2015, *Mon. Not. Roy. Astron. Soc.*, 453, 128
- Lloyd-Ronning, N. M., Fryer, C. L., & Ramirez-Ruiz, E. 2002, *Astrophys. J.*, 574, 554
- Longo, M. J. 1988, *Physical Review Letters*, 60, 173
- Lü, H.-J., Liang, E.-W., Zhang, B.-B., & Zhang, B. 2010, *Astrophys. J.*, 725, 1965
- Luzzi, G., Shimon, M., Lamagna, L., Rephaeli, Y., De Petris, M., Conte, A., De Gregori, S., & Battistelli, E. S. 2009, *Astrophys. J.*, 705, 1122
- Lynden-Bell, D. 1971, *Mon. Not. Roy. Astron. Soc.*, 155, 95
- MacFadyen, A. I., & Woosley, S. E. 1999, *Astrophys. J.*, 524, 262
- Macpherson, D., Coward, D. M., & Zadnik, M. G. 2013, *Astrophys. J.*, 779, 73
- Maio, U., Ciardi, B., Dolag, K., Tornatore, L., & Khochfar, S. 2010, *Mon. Not. Roy. Astron. Soc.*, 407, 1003
- Mazzali, P. A., Deng, J., Nomoto, K., Sauer, D. N., Pian, E., Tominaga, N., Tanaka, M., Maeda, K., & Filippenko, A. V. 2006, *Natur.*, 442, 1018
- McKee, C. F., & Tan, J. C. 2008, *Astrophys. J.*, 681, 771
- McMillan, P. J. 2011, *Mon. Not. Roy. Astron. Soc.*, 414, 2446

- Mesler, R. A., Whalen, D. J., Smidt, J., Fryer, C. L., Lloyd-Ronning, N. M., & Pihlström, Y. M. 2014, *Astrophys. J.*, 787, 91
- Mészáros, P. 2006, *Reports on Progress in Physics*, 69, 2259
- Mészáros, P., & Rees, M. J. 2010, *Astrophys. J.*, 715, 967
- Molaro, P., Centurión, M., Whitmore, J. B., Evans, T. M., Murphy, M. T., Agafonova, I. I., Bonifacio, P., D’Odorico, S., Levshakov, S. A., Lopez, S., Martins, C. J. A. P., Petitjean, P., Rahmani, H., Reimers, D., Srianand, R., Vladilo, G., & Wendt, M. 2013, *Astron. Astrophys.*, 555, A68
- Molaro, P., Levshakov, S. A., Dessauges-Zavadsky, M., & D’Odorico, S. 2002, *Astron. Astrophys.*, 381, L64
- Mörtsell, E., & Sollerman, J. 2005, *J. Cosmol. Astropart. P.*, 6, 9
- Murphy, M. T., Webb, J. K., & Flambaum, V. V. 2003, *Mon. Not. Roy. Astron. Soc.*, 345, 609
- Nagakura, H., Ito, H., Kiuchi, K., & Yamada, S. 2011, *Astrophys. J.*, 731, 80
- Nakauchi, D., Suwa, Y., Sakamoto, T., Kashiyama, K., & Nakamura, T. 2012, *Astrophys. J.*, 759, 128
- Natarajan, P., Albanna, B., Hjorth, J., Ramirez-Ruiz, E., Tanvir, N., & Wijers, R. 2005, *Mon. Not. Roy. Astron. Soc.*, 364, L8
- Niino, Y. 2011, *Mon. Not. Roy. Astron. Soc.*, 417, 567
- Norris, J. P., Marani, G. F., & Bonnell, J. T. 2000, *Astrophys. J.*, 534, 248
- Noterdaeme, P., Petitjean, P., Ledoux, C., López, S., Srianand, R., & Vergani, S. D. 2010, *Astron. Astrophys.*, 523, A80
- Oguri, M., & Takahashi, K. 2006, *Phys. Rev. D*, 73, 123002
- Oh, S. P. 2002, *Mon. Not. Roy. Astron. Soc.*, 336, 1021
- Oppenheimer, B. D., Davé, R., & Finlator, K. 2009, *Mon. Not. Roy. Astron. Soc.*, 396, 729
- Paul, J., Wei, J., Basa, S., & Zhang, S.-N. 2011, *Comptes Rendus Physique*, 12, 298
- Perlmutter, S., Aldering, G., Goldhaber, G., Knop, R. A., Nugent, P., Castro, P. G., Deustua, S., Fabbro, S., Goobar, A., Groom, D. E., Hook, I. M., Kim, A. G., Kim, M. Y., Lee, J. C., Nunes, N. J., Pain, R., Pennypacker, C. R., Quimby, R., Lidman, C., Ellis, R. S., Irwin, M., McMahon, R. G., Ruiz-Lapuente, P., Walton, N., Schaefer, B., Boyle, B. J., Filippenko, A. V., Matheson, T., Fruchter, A. S., Panagia, N., Newberg, H. J. M., Couch, W. J., & Project, T. S. C. 1999, *Astrophys. J.*, 517, 565
- Petitjean, P., & Vergani, S. D. 2011, *Comptes Rendus Physique*, 12, 288
- Pian, E., Mazzali, P. A., Masetti, N., Ferrero, P., Klose, S., Palazzi, E., Ramirez-Ruiz, E., Woosley, S. E., Kouveliotou, C., Deng, J., Filippenko, A. V., Foley, R. J., Fynbo, J. P. U., Kann, D. A., Li, W., Hjorth, J., Nomoto, K., Patat, F., Sauer, D. N., Sollerman, J., Vreeswijk, P. M., Guenther, E. W., Levan, A., O’Brien, P., Tanvir, N. R., Wijers, R. A. M. J., Dumas, C., Hainaut, O., Wong, D. S., Baade, D., Wang, L., Amati, L., Cappellaro, E., Castro-Tirado, A. J., Ellison, S., Frontera, F., Fruchter, A. S., Greiner, J., Kawabata, K., Ledoux, C., Maeda, K., Möller, P., Nicastro, L., Rol, E., & Starling, R. 2006, *Natur.*, 442, 1011
- Porciani, C., & Madau, P. 2001, *Astrophys. J.*, 548, 522
- Price, P. A., Songaila, A., Cowie, L. L., Bell Burnell, J., Berger, E., Cucchiara, A., Fox, D. B., Hook, I., Kulkarni, S. R., Penprase, B., Roth, K. C., & Schmidt, B. 2007, *Astrophys. J. Lett.*, 663, L57
- Prochaska, J. X., Chen, H.-W., Dessauges-Zavadsky, M., & Bloom, J. S. 2007, *Astrophys. J.*, 666, 267
- Prochaska, J. X., Sheffer, Y., Perley, D. A., Bloom, J. S., Lopez, L. A., Dessauges-Zavadsky, M., Chen, H.-W., Filippenko, A. V., Ganeshalingam, M., Li, W., Miller, A. A., & Starr, D. 2009, *Astrophys. J. Lett.*, 691, L27
- Qi, S., & Lu, T. 2010, *Astrophys. J.*, 717, 1274
- Qi, S., Lu, T., & Wang, F.-Y. 2009, *Mon. Not. Roy. Astron. Soc.*, 398, L78
- Qi, S., Wang, F.-Y., & Lu, T. 2008a, *Astron. Astrophys.*, 483, 49
- . 2008b, *Astron. Astrophys.*, 487, 853
- Qin, S.-F., Liang, E.-W., Lu, R.-J., Wei, J.-Y., & Zhang, S.-N. 2010, *Mon. Not. Roy. Astron. Soc.*, 406, 558
- Rahmani, H., Wendt, M., Srianand, R., Noterdaeme, P., Petitjean, P., Molaro, P., Whitmore, J. B., Murphy, M. T., Centurion, M., Fathivavsari, H., D’Odorico, S., Evans, T. M., Levshakov, S. A., Lopez, S., Martins, C. J. A. P., Reimers, D., & Vladilo, G. 2013, *Mon. Not. Roy. Astron. Soc.*, 435, 861
- Rhoads, J. E. 1997, *Astrophys. J. Lett.*, 487, L1

- Riess, A. G., Filippenko, A. V., Challis, P., Clocchiatti, A., Diercks, A., Garnavich, P. M., Gilliland, R. L., Hogan, C. J., Jha, S., Kirshner, R. P., Leibundgut, B., Phillips, M. M., Reiss, D., Schmidt, B. P., Schommer, R. A., Smith, R. C., Spyromilio, J., Stubbs, C., Suntzeff, N. B., & Tonry, J. 1998, *Astron. J.*, 116, 1009
- Robertson, B. E., & Ellis, R. S. 2012, *Astrophys. J.*, 744, 95
- Salvaterra, R., Campana, S., Vergani, S. D., Covino, S., D'Avanzo, P., Fugazza, D., Ghirlanda, G., Ghisellini, G., Melandri, A., Nava, L., Sbarufatti, B., Flores, H., Piranomonte, S., & Tagliaferri, G. 2012, *Astrophys. J.*, 749, 68
- Salvaterra, R., & Chincarini, G. 2007, *Astrophys. J. Lett.*, 656, L49
- Salvaterra, R., Della Valle, M., Campana, S., Chincarini, G., Covino, S., D'Avanzo, P., Fernández-Soto, A., Guidorzi, C., Mannucci, F., Margutti, R., Thöne, C. C., Antonelli, L. A., Barthelmy, S. D., de Pasquale, M., D'Elia, V., Fiore, F., Fugazza, D., Hunt, L. K., Maiorano, E., Marinoni, S., Marshall, F. E., Molinari, E., Nousek, J., Pian, E., Racusin, J. L., Stella, L., Amati, L., Andreuzzi, G., Cusumano, G., Fenimore, E. E., Ferrero, P., Giommi, P., Guetta, D., Holland, S. T., Hurley, K., Israel, G. L., Mao, J., Markwardt, C. B., Masetti, N., Pagani, C., Palazzi, E., Palmer, D. M., Piranomonte, S., Tagliaferri, G., & Testa, V. 2009, *Natur.*, 461, 1258
- Sari, R. 1999, *Astrophys. J. Lett.*, 524, L43
- Savaglio, S., Glazebrook, K., Le Borgne, D., Juneau, S., Abraham, R. G., Chen, H.-W., Cramp-ton, D., McCarthy, P. J., Carlberg, R. G., Marzke, R. O., Roth, K., Jørgensen, I., & Murowinski, R. 2005, *Astrophys. J.*, 635, 260
- Schaefer, B. E. 2007, *Astrophys. J.*, 660, 16
- Schaefer, B. E., Gerardy, C. L., Höflich, P., Panaitescu, A., Quimby, R., Mader, J., Hill, G. J., Kumar, P., Wheeler, J. C., Eracleous, M., Sigurdsson, S., Mészáros, P., Zhang, B., Wang, L., Hessman, F. V., & Petrosian, V. 2003, *Astrophys. J.*, 588, 387
- Schmidt, M. 1999, *Astrophys. J. Lett.*, 523, L117
- Schneider, R., Ferrara, A., Natarajan, P., & Omukai, K. 2002, *Astrophys. J.*, 571, 30
- Schneider, R., Omukai, K., Inoue, A. K., & Ferrara, A. 2006, *Mon. Not. Roy. Astron. Soc.*, 369, 1437
- Shapiro, I. I. 1964, *Physical Review Letters*, 13, 789
- Shu, F. H., Lizano, S., Galli, D., Cantó, J., & Laughlin, G. 2002, *Astrophys. J.*, 580, 969
- Sivaram, C. 1999, *Bulletin of the Astronomical Society of India*, 27, 627
- Soderberg, A. M., Kulkarni, S. R., Nakar, E., Berger, E., Cameron, P. B., Fox, D. B., Frail, D., Gal-Yam, A., Sari, R., Cenko, S. B., Kasliwal, M., Chevalier, R. A., Piran, T., Price, P. A., Schmidt, B. P., Pooley, G., Moon, D.-S., Penprase, B. E., Ofek, E., Rau, A., Gehrels, N., Nousek, J. A., Burrows, D. N., Persson, S. E., & McCarthy, P. J. 2006, *Natur.*, 442, 1014
- Sollerman, J., Östlin, G., Fynbo, J. P. U., Hjorth, J., Fruchter, A., & Pedersen, K. 2005, *New Astron.*, 11, 103
- Spergel, D. N., Verde, L., Peiris, H. V., Komatsu, E., Nolta, M. R., Bennett, C. L., Halpern, M., Hinshaw, G., Jarosik, N., Kogut, A., Limon, M., Meyer, S. S., Page, L., Tucker, G. S., Weiland, J. L., Wollack, E., & Wright, E. L. 2003, *Astrophys. J. Suppl.*, 148, 175
- Srianand, R., Chand, H., Petitjean, P., & Aracil, B. 2004, *Physical Review Letters*, 92, 121302
- 2007, *Physical Review Letters*, 99, 239002
- Srianand, R., Gupta, N., Petitjean, P., Noterdaeme, P., Ledoux, C., Salter, C. J., & Saikia, D. J. 2012, *Mon. Not. Roy. Astron. Soc.*, 421, 651
- Srianand, R., Noterdaeme, P., Ledoux, C., & Petitjean, P. 2008, *Astron. Astrophys.*, 482, L39
- Stacy, A., Bromm, V., & Loeb, A. 2011, *Mon. Not. Roy. Astron. Soc.*, 413, 543
- Stacy, A., Greif, T. H., & Bromm, V. 2012, *Mon. Not. Roy. Astron. Soc.*, 422, 290
- Stanek, K. Z., Gnedin, O. Y., Beacom, J. F., Gould, A. P., Johnson, J. A., Kollmeier, J. A., Modjaz, M., Pinsonneault, M. H., Pogge, R., & Weinberg, D. H. 2006, *Acta Astronomy*, 56, 333
- Stanek, K. Z., Matheson, T., Garnavich, P. M., Martini, P., Berlind, P., Caldwell, N., Challis, P., Brown, W. R., Schild, R., Krisciunas, K., Calkins, M. L., Lee, J. C., Hathi, N., Jansen, R. A., Windhorst, R., Echevarria, L., Eisenstein, D. J., Pindor, B., Olszewski, E. W., Harding, P., Holland, S. T., & Bersier, D. 2003, *Astrophys. J. Lett.*, 591, L17
- Svensson, K. M., Levan, A. J., Tanvir, N. R., Fruchter, A. S., & Strolger, L.-G. 2010, *Mon. Not. Roy. Astron. Soc.*, 405, 57
- Tan, W.-W., Cao, X.-F., & Yu, Y.-W. 2013, *Astrophys. J. Lett.*, 772, L8
- Tegmark, M., Silk, J., Rees, M. J., Blanchard, A., Abel, T., & Palla, F. 1997, *Astrophys. J.*, 474, 1

- Toma, K., Sakamoto, T., & Mészáros, P. 2011, *Astrophys. J.*, 731, 127
- Totani, T. 1997, *Astrophys. J. Lett.*, 486, L71
- Uzan, J.-P., Aghanim, N., & Mellier, Y. 2004, *Phys. Rev. D*, 70, 083533
- Valageas, P. 2000, *Astron. Astrophys.*, 354, 767
- Vasileiou, V., Jacholkowska, A., Piron, F., Bolmont, J., Couturier, C., Granot, J., Stecker, F. W., Cohen-Tanugi, J., & Longo, F. 2013, *Phys. Rev. D*, 87, 122001
- Vink, J. S., & de Koter, A. 2005, *Astron. Astrophys.*, 442, 587
- Virgili, F. J., Zhang, B., Nagamine, K., & Choi, J.-H. 2011, *Mon. Not. Roy. Astron. Soc.*, 417, 3025
- Visser, M. 2004, *Classical and Quantum Gravity*, 21, 2603
- Vitagliano, V., Xia, J.-Q., Liberati, S., & Viel, M. 2010, *J. Cosmol. Astropart. P.*, 3, 5
- Vreeswijk, P. M., Ledoux, C., Smette, A., Ellison, S. L., Jaunsen, A. O., Andersen, M. I., Fruchter, A. S., Fynbo, J. P. U., Hjorth, J., Kaufer, A., Møller, P., Petitjean, P., Savaglio, S., & Wijers, R. A. M. J. 2007, *Astron. Astrophys.*, 468, 83
- Wanderman, D., & Piran, T. 2010, *Mon. Not. Roy. Astron. Soc.*, 406, 1944
- . 2015, *Mon. Not. Roy. Astron. Soc.*, 448, 3026
- Wang, F. Y. 2012, *Astron. Astrophys.*, 543, A91
- . 2013, *Astron. Astrophys.*, 556, A90
- Wang, F. Y., Bromm, V., Greif, T. H., Stacy, A., Dai, Z. G., Loeb, A., & Cheng, K. S. 2012, *Astrophys. J.*, 760, 27
- Wang, F.-Y., & Dai, Z.-G. 2006a, *Chin. J. Astron. Astr.*, 6, 561
- . 2006b, *Chin. J. Astron. Astr.*, 6, 561
- Wang, F. Y., & Dai, Z. G. 2006c, *Mon. Not. Roy. Astron. Soc.*, 368, 371
- . 2009, *Mon. Not. Roy. Astron. Soc.*, 400, L10
- . 2011a, *Astrophys. J. Lett.*, 727, L34
- . 2011b, *Astron. Astrophys.*, 536, A96
- . 2013, *Nature Physics*, 9, 465
- . 2014a, *Phys. Rev. D*, 89, 023004
- . 2014b, *Astrophys. J. Suppl.*, 213, 15
- Wang, F. Y., Dai, Z. G., & Liang, E. W. 2015, *New Atron. Rev.*, 67, 1
- Wang, F. Y., Dai, Z. G., & Qi, S. 2009, *Astron. Astrophys.*, 507, 53
- Wang, F. Y., Dai, Z. G., & Zhu, Z.-H. 2007, *Astrophys. J.*, 667, 1
- Wang, F.-Y., Qi, S., & Dai, Z.-G. 2011a, *Mon. Not. Roy. Astron. Soc.*, 415, 3423
- Wang, F. Y., Yi, S. X., & Dai, Z. G. 2014, *Astrophys. J. Lett.*, 786, L8
- Wang, J. S., & Wang, F. Y. 2014, *Astron. Astrophys.*, 564, A137
- Wang, Y. 2008, *Phys. Rev. D*, 78, 123532
- Wang, Y., Fan, Y.-Z., & Wei, D.-M. 2011b, *Physical Review Letters*, 106, 259001
- Wei, H. 2010, *J. Cosmol. Astropart. P.*, 8, 20
- Wei, J.-J., Ma, Q.-B., & Wu, X.-F. 2015, *Advances in Astronomy*, 2015, 20
- Wei, J.-J., Wu, X.-F., & Melia, F. 2013, *Astrophys. J.*, 772, 43
- Wei, J.-J., Wu, X.-F., Melia, F., Wei, D.-M., & Feng, L.-L. 2014, *Mon. Not. Roy. Astron. Soc.*, 439, 3329
- Wijers, R. A. M. J., Bloom, J. S., Bagla, J. S., & Natarajan, P. 1998, *Mon. Not. Roy. Astron. Soc.*, 294, L13
- Will, C. M. 2006, *Living Reviews in Relativity*, 9, 3
- . 2014, *Living Reviews in Relativity*, 17, 4
- Wolf, C., & Podsiadlowski, P. 2007, *Mon. Not. Roy. Astron. Soc.*, 375, 1049
- Woodsley, S. E. 1993, *Astrophys. J.*, 405, 273
- Woodsley, S. E., & Bloom, J. S. 2006, *Annu. Rev. Astron. Astr.*, 44, 507
- Woodsley, S. E., & Heger, A. 2006, *Astrophys. J.*, 637, 914
- Woodsley, S. E., & Weaver, T. A. 1995, *Astrophys. J. Suppl.*, 101, 181
- Wu, S.-W., Xu, D., Zhang, F.-W., & Wei, D.-M. 2012, *Mon. Not. Roy. Astron. Soc.*, 423, 2627
- Wyithe, J. S. B., & Loeb, A. 2003, *Astrophys. J.*, 586, 693
- Xia, J.-Q., Vitagliano, V., Liberati, S., & Viel, M. 2012, *Phys. Rev. D*, 85, 043520
- Xu, C. Y., & Wei, D. M. 2008, *Acta Astronomica Sinica*, 49, 387
- Xu, D., Dai, Z. G., & Liang, E. W. 2005, *Astrophys. J.*, 633, 603
- Yonetoku, D., Murakami, T., Nakamura, T., Yamazaki, R., Inoue, A. K., & Ioka, K. 2004, *Astrophys. J.*, 609, 935
- Yoon, S.-C., & Langer, N. 2005, *Astron. Astrophys.*, 443, 643
- Yoon, S.-C., Langer, N., & Norman, C. 2006, *Astron. Astrophys.*, 460, 199

- Yoshida, N., Abel, T., Hernquist, L., & Sugiyama, N. 2003, *Astrophys. J.*, 592, 645
- Yu, B., Qi, S., & Lu, T. 2009, *Astrophys. J. Lett.*, 705, L15
- Yu, Y.-W., Cheng, K. S., Chu, M. C., & Yeung, S. 2012, *J. Cosmol. Astropart. P.*, 7, 23
- Yüksel, H., & Kistler, M. D. 2007, *Phys. Rev. D*, 75, 083004
- Yüksel, H., Kistler, M. D., Beacom, J. F., & Hopkins, A. M. 2008, *Astrophys. J. Lett.*, 683, L5
- Zhang, B. 2006, *Natur.*, 444, 1010
- . 2007, *Chin. J. Astron. Astr.*, 7, 1
- . 2014, *International Journal of Modern Physics D*, 23, 30002
- Zhang, B., Zhang, B.-B., Virgili, F. J., Liang, E.-W., Kann, D. A., Wu, X.-F., Proga, D., Lv, H.-J., Toma, K., Mészáros, P., Burrows, D. N., Roming, P. W. A., & Gehrels, N. 2009, *Astrophys. J.*, 703, 1696
- Zhang, S., & Ma, B.-Q. 2015, *Astroparticle Physics*, 61, 108
- Zhao, G.-B., Crittenden, R. G., Pogosian, L., & Zhang, X. 2012, *Physical Review Letters*, 109, 171301